

**A Simplified Method for the Repetition Rate Stabilization  
of Modelocked Lasers: A PDH-based Technique**

by

**Luke Charbonneau**

B.A., Physics, University of Colorado, 2016

A thesis submitted to the  
Faculty of the Graduate School of the  
University of Colorado in partial fulfillment  
of the requirements for the degree of  
Master of Physics  
Department of Physics  
2016

This thesis entitled:  
A Simplified Method for the Repetition Rate Stabilization of Modelocked Lasers: A  
PDH-based Technique  
written by Luke Charbonneau  
has been approved for the Department of Physics

---

Prof. Thomas Schibli

---

Prof. Markus Raschke

---

Prof. Steven Pollock

Date \_\_\_\_\_

The final copy of this thesis has been examined by the signatories, and we find that both the content and the form meet acceptable presentation standards of scholarly work in the above mentioned discipline.

Charbonneau, Luke (M.S., Physics)

A Simplified Method for the Repetition Rate Stabilization of Modelocked Lasers: A PDH-based Technique

Thesis directed by Prof. Thomas Schibli

High-quality ultrashort pulses of light generated by solid-state modelocked femtosecond lasers have become increasingly recognized in recent years as indispensable tools for precision spectroscopy and frequency metrology due to their ability to form optical frequency combs (OFC) over a wide spectral range. Furthermore, of particular interest to many fields is an OFC's ability to produce microwave signals with a high degree of spectral purity - ultimately limited by the phase noise of the modelocked laser used to generate the comb. As a result, several effective techniques have been developed for stabilizing modelocked lasers, but they often involve a high degree of complexity and cost. In this thesis, a simplified modelocked laser stabilization scheme based on the famous Pound, Drever, Hall continuous-wave laser stabilization technique is demonstrated, which was capable of significant phase noise suppression up to at least a 1.1 kHz offset frequency. By essentially PDH-locking the repetition rate of a solid-state Er:Yb modelocked laser to a single reference cavity, the integrated timing jitter from 100 Hz - 10 MHz was reduced nearly four-fold, without the need for complex and delicate RF or CW laser references. This simplified and robust method for long-term repetition rate stabilization furthers the potential for the development of inexpensive, low-noise, field deployable solid-state modelocked laser-generated frequency combs - a market currently dominated by their fiber-based counterparts.

## **Dedication**

To my fantastic parents, Lauren and Armand Charbonneau.

## Acknowledgements

I would first like to thank all of the members of the Schibli Lab, who have all helped me in some way to become a better researcher. In particular, Professor Thomas Schibli and Dr. Chien-Chung Lee, who have always taken the time, despite how busy they always were, to answer my questions thoroughly and teach me lab techniques. I would also like to thank my friend and colleague, Tyko Shoji, for the many enlightening discussions we have had about various experimental techniques and theoretical concepts (as well as being a worthy opponent in the perpetual battle for the best measurement devices in the lab). Furthermore, I would like to thank Maithreyi Gopalakrishnan for working with me during the many rigorous courses that are an integral part of a graduate physics education (particularly one inspired by the late John David Jackson comes to mind). Lastly, a thank you to Liangyu Chen, a talented undergraduate in the Schibli lab who helped me out in the early stages of the project. There are many others, but I could probably write another thesis containing the names of every person at the University of Colorado who has enabled my academic success. Therefore, a heartfelt thank you to everyone here in Boulder who has helped me along the way.

## Contents

### Chapter

<b>1</b>	<b>Introduction</b>	<b>1</b>
1.1	Motivation for low-noise modelocked Lasers . . . . .	1
1.1.1	Metrology . . . . .	3
1.1.2	Microwave Generation . . . . .	3
1.1.3	Spectroscopy . . . . .	5
<b>2</b>	<b>Noise in Lasers</b>	<b>8</b>
2.1	Types of Noise in Continuous Wave Lasers . . . . .	8
2.1.1	Intensity Noise . . . . .	8
2.1.2	Phase Noise . . . . .	12
2.2	Noise in Modelocked Lasers . . . . .	15
2.2.1	From Waves to Pulses: A Brief Introduction to Passive Modelocking .	16
2.2.2	Timing Jitter . . . . .	18
2.3	Beam Pointing Fluctuations . . . . .	24
2.4	Noise in Lasers vs Passive Reference Cavities . . . . .	25
2.4.1	Cavity Finesse . . . . .	26
2.4.2	Passive Optical Cavity Resonances . . . . .	27
<b>3</b>	<b>PDH-Based Repetition Rate Stabilization Technique</b>	<b>29</b>
3.1	Theory: Early Laser Stabilization Techniques . . . . .	29

3.1.1	The Pound, Drever, Hall (PDH) Technique . . . . .	30
3.1.2	The Hänsch-Couillaud Technique . . . . .	37
3.1.3	Stabilization Techniques for Modelocked lasers . . . . .	42
3.2	Experimental Setup . . . . .	46
3.2.1	500 MHz Modelocked Laser . . . . .	47
3.2.2	Electro-optic Modulator . . . . .	50
3.2.3	Stable Reference Cavity . . . . .	51
3.2.4	Environmental Isolation . . . . .	53
3.2.5	Electronics . . . . .	53
3.2.6	500 MHz to 1 GHz Interleaver . . . . .	55
<b>4</b>	<b>Results</b>	<b>57</b>
4.1	Lock Performance . . . . .	57
4.2	Phase Noise Measurement . . . . .	58
4.2.1	Phase Noise Measurement Setup . . . . .	59
4.2.2	Phase Noise Measurement Results . . . . .	63
<b>5</b>	<b>Conclusion and Future Outlook</b>	<b>67</b>
5.0.1	Conclusion . . . . .	67
5.0.2	Future Study . . . . .	68
	<b>References</b>	<b>70</b>
	<b>Appendix</b>	
<b>A</b>	<b>Kigre Inc. Erbium-doped Ytterbium Glass, QX/Er Datasheet</b>	<b>73</b>
<b>B</b>	<b>Fiber-Based Lithium Niobate EOM-PM Datasheet</b>	<b>74</b>

**C Layertec Mirror Dielectric Coating Datasheets****75**



## Figures

### Figure

1.1	Femtosecond comb divided down to microwave frequency . . . . .	5
1.2	Calibration of an astronomical spectrometer using a femtosecond comb . . .	7
2.1	A generic solid state laser power spectral density intensity noise spectrum . .	10
2.2	An example of a Self-Heterodyne Setup . . . . .	15
2.3	Gains, losses and optical power over time in a passively modelocked laser . .	16
2.4	Illustration of addition of many longitudinal cavity modes . . . . .	18
2.5	A visual representation of timing jitter . . . . .	19
3.1	Outline of a Pound, Drever, Hall (PDH) stabilization experimental setup . .	31
3.2	Reflection coefficient from a Fabry-Perot cavity in the complex plane . . . .	32
3.3	The PDH error signal for a high modulation frequency . . . . .	35
3.4	The Hänsch-Couillaud setup . . . . .	38
3.5	The Hänsch-Couillaud error signal . . . . .	41
3.6	The self-referencing (f-2f) scheme setup . . . . .	43
3.7	The differential frequency comb lock setup . . . . .	45
3.8	A diagram of the experimental setup . . . . .	47
3.9	ABCD calculation screen shot for 500 MHz modelocked laser . . . . .	48
3.10	The experimental environmental isolation setup . . . . .	54
3.11	The circuit diagram for the PI servo loop filter . . . . .	56

4.1	Passive cavity resonances with the electro-optic phase modulator turned off .	58
4.2	Passive cavity resonances with the electro-optic phase modulator turned on .	59
4.3	The experimental PDH error signal . . . . .	60
4.4	The transmission signal through the reference cavity with lock engaged . . .	61
4.5	A block diagram for the phase noise measurement scheme described in section	
4.2.1	. . . . .	65
4.6	The phase noise measurement results using the method described in section 4.2.1	66

# Chapter 1

## Introduction

### 1.1 Motivation for low-noise modelocked Lasers

Modelocked lasers have revolutionized the field of ultrafast optics since they were first demonstrated in 1964 by Hargrove et al [1]. Modelocked lasers produce trains of light pulses which are very evenly-spaced in the time domain, which are useful for a wide range of applications - several of which will be enumerated in the following section. Like all optical systems, modelocked lasers suffer from several types of noise which originate from various sources (these noise sources will be discussed in detail in chapter 2). The type of noise of particular interest for this thesis is known as *timing jitter*. Timing jitter describes the degree of irregularity in the time domain spacing of pulses in a modelocked lasers' output. Therefore, for an ideal modelocked laser with zero timing jitter, one would measure a fixed time interval between the detection of any pulse and a subsequent pulse. Timing jitter is particularly important to minimize for many applications such as optical data transmission, optical sampling measurements and experiments involving two synchronized lasers [2]. Furthermore, stabilized modelocked lasers form the basis of an important optical device known as a *femtosecond comb*. Femtosecond combs generated by modelocked lasers are a special class of frequency combs, which can be generated via other techniques such as amplitude modulation and four-wave mixing. However, comb generation with femtosecond modelocked lasers provides several advantages over other techniques and will be the main focus of this thesis. Femtosecond combs can be thought of as the Fourier transform of a

stable train of pulses from a modelocked laser. That is, in the time domain, the output of a modelocked laser consists of very short, evenly-spaced packets of light. However, the same output in the frequency domain appears as a wide spectrum of evenly-spaced spectral components (see the optical spectrum in figure 1.1). Furthermore, the shorter the pulses produced in the time domain, the more spectral components or "comb teeth" that will be at an experimentalist's disposal in the frequency domain. Due to the very evenly-spaced nature of the spectral components of an optical frequency comb, describing the position of any comb tooth (i.e. a single frequency/spectral component) is fairly straightforward. The elementary mathematics describing a femtosecond comb in the frequency domain is shown below:

$$f(n) = f_0 + nf_r \quad (1.1)$$

where  $f_r$  is the pulse repetition rate of the modelocked laser producing the comb,  $n$  is an integer that represents a specific comb "tooth" (i.e. frequency component) and  $f_0$  is a frequency offset known as the *carrier-envelope offset frequency*.

The *carrier envelope* describes the position of a pulse in the time domain, whereas the *carrier* is the relatively fast, sinusoidal variation of the electric field within the pulse (an example of a carrier and carrier envelope can be seen on the left-hand side of figure 1.2). In general, when a pulse travels through a medium, chromatic dispersion (in addition to nonlinear effects) occurs and causes a difference between the phase and group velocity of the pulses. This leads to a shift in the relative phase between the carrier envelope and the carrier phase of the pulse which, per laser resonator round-trip, is represented by the *carrier-envelope offset phase*,  $\Delta\phi_{CEO}$  [3]. This leads to the aforementioned carrier envelope offset frequency,  $f_0$ , described by [3]:

$$f_0 = \frac{\Delta\phi_{CEO} \bmod 2\pi}{2\pi} f_r \quad (1.2)$$

where the  $\bmod 2\pi$  term demonstrates that only the modulus  $2\pi$  phase shift between the carrier

envelope and carrier phase, per round-trip, is relevant. The measurement and stabilization of this offset frequency is discussed in chapter 3 of this thesis.

The teeth of a frequency comb, if properly stabilized, are useful for a wide variety of applications involving relative or even absolute frequency measurement. Thus, the motivation for developing techniques to better stabilize femtosecond modelocked lasers used for the generation of frequency combs is established.

### 1.1.1 Metrology

Femtosecond combs produced by a single modelocked laser have greatly simplified the implementation of accurate and reliable optical frequency measurements by eliminating the need for a complex optical frequency chain. Femtosecond combs which have one degree of freedom stabilized, usually  $f_r$  - the pulse repetition frequency, can be used to make relative optical frequency measurements. Furthermore, if the carrier envelope offset frequency,  $f_0$ , is also properly stabilized then the comb may be used as an *absolute* frequency reference. With the precise level of optical frequency measurement that stabilized combs provide, advances in the measurement of fundamental physical phenomena have become more feasible. Specifically, improvements in the measured value of the speed of light, measurements of the Lamb shift predicted by quantum electrodynamics, refinements of the measured value of the fine structure constant and more rigorous tests of the theory of special relativity are significantly simplified by the ability of stabilized femtosecond combs to span a wide bandwidth [4].

### 1.1.2 Microwave Generation

Low phase noise microwave signals with high spectral purity are currently desired to improve the precision of clocks, metrology, radar and communications, in addition to a wide range of other potential applications [5]. Cryogenic sapphire microwave oscillators can be used to generate these low phase noise signals [6], but require a relatively large amount of space and costly equipment. To avoid these drawbacks, frequency combs can be used to

divide a low noise optical oscillator down to microwave frequencies - effectively transferring the relatively high stability of an optical cavity to the microwave domain [ 5]. Furthermore, in this type of technique for low phase noise microwave generation, the noise present in the final microwave signal is ultimately determined by the stability of the frequency comb produced by a modelocked laser (figure 1.1) [7]. Thus, it is desirable for this type of microwave generation technique to use the lowest noise, i.e. best stabilized, frequency comb possible. Stabilized femtosecond combs are also of particular interest to atomic clock makers. Frequency standards for units of time, e.g. a second, are currently defined by microwave transitions within a Cesium atom [4]. If the Ramsey separated field method and the condition that the interrogation time,  $T_r$ , is shorter than the lifetime of the transition used are assumed, then the fractional frequency instability can be described as [4]:

$$\sigma_y(\tau) = \frac{\delta\nu}{\nu_0} = \frac{1}{\omega_0 \sqrt{NT_r\tau}} \quad (1.3)$$

where  $\omega_0$  is the clock transition frequency used and  $\tau$  is the averaging time. From 1.3, it can be clearly seen that using a clock transition frequency in the optical domain allows for a higher stability (i.e. lower fractional frequency instability) than using a clock transition frequency in the microwave domain (as is commonly done in most atomic clocks today). In fact, the tracking of the most advanced femtosecond comb systems exceeds the stability of current optical frequency standards, therefore, it is expected that the stability of the optical clock will be comparable to the optical standard itself [4]. Thus, the development of even more stable femtosecond combs will almost surely enable the future drive towards even more precise atomic frequency standards. Furthermore, the ability to produce a low noise femtosecond comb, and hence provide ready access to any combination of optical frequencies, opens up the possibility of creating optical synthesizers capable of creating any arbitrary pulse of light [4].

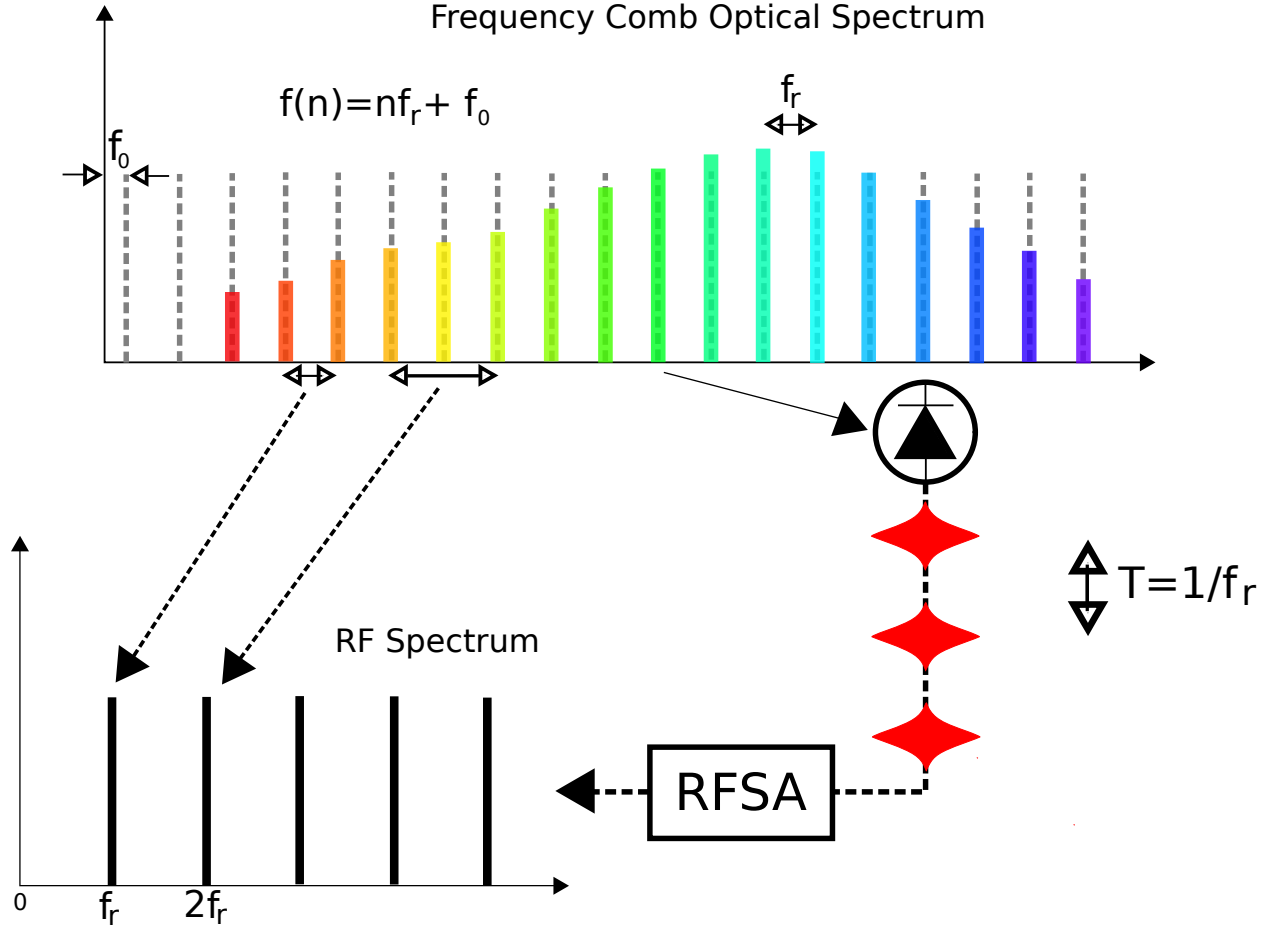


Figure 1.1: A femtosecond comb divided down to microwave frequency for the generation of a 10 GHz low noise microwave signal.

### 1.1.3 Spectroscopy

Perhaps one of the most important applications of femtosecond combs is in the extensive and multifaceted field of spectroscopy. Femtosecond light pulses produced by stabilized modelocked lasers have allowed for the spectroscopic measurement of time-resolved fast dynamics, as well as unprecedented precision and flexibility in spectroscopic measurements of atomic and molecular structural phenomena [4]. The ability of a single femtosecond comb to span a large spectral region allows for the uniform detection and measurement of small changes in molecular structure with unprecedented precision and greatly decreased complexity [4]. For example, in 2005, Marian et al. used direct frequency comb spectroscopy

to determine the absolute frequency of the two-photon 5S-7S transition in  $^{87}\text{Rb}$ , which was previously undetermined [8]. With this particular measurement, Marian et al. were able to show that prior knowledge of the atomic transition to be measured is not necessary for this technique, thus demonstrating the great flexibility of using femtosecond combs for direct spectroscopic measurements [8]. Furthermore, femtosecond combs can be used to precisely calibrate astronomical spectrometers. There exists a paramount and inconclusively solved question in astronomy which has drawn the attention of greats such as Einstein and Hubble: what exactly is the current expansion rate of the universe? Although this question may simply appear to be a manifestation of astronomers fastidiousness for precise data, in actuality, the answer has far-reaching consequences for modern astronomical theories. In fact, the theory of dark matter and even a pillar of modern astronomy - the Copernican principle - hang in the balance as astronomers search for a way to precisely determine this expansion rate. Unfortunately, our current astronomical instruments are thus far incapable of making a precise-enough red shift measurement to accurately determine this rate and the current prediction that the expansion is accelerating on the order of  $1\frac{\text{cm}}{\text{s}}$  per year is based solely on the distances of type 1a supernovae [9]. Confirming (or repudiating) these predictions through the direct measurement of changes in the red shift of far-away celestial objects would topple (or vindicate) alternative theories regarding the expansion and energy composition of the universe [9]. The best astronomical spectrometers available offer long term stabilities which are, in theory, several times more stable than would be required to make this measurement. However, one large limiting factor of the effectiveness of these devices is the ability to calibrate them accurately. The classical method of calibrating these spectrometers is to superimpose the light collected from the telescope onto a reference spectrum. This method of calibration limits the precision of the instruments due to repeatability issues and errors in the reference spectra [9]. A better method of calibration was first utilized by Steinmetz et al. in 2008, in which a stabilized femtosecond comb is used to form an ultra-precise frequency ruler which is then used to calibrate an astronomical spectrometer (see figure 1.2) [10]. This



method of calibration allowed for an equivalent Doppler precision of  $\sim 9$  meters per second at  $\sim 1.5$  micrometers beyond the previous best calibration accuracy [10]. Therefore, the use of stabilized femtosecond combs will likely soon allow astronomers to confirm the predictions of the universe's expansion rate currently based solely on 1a supernovae distances.

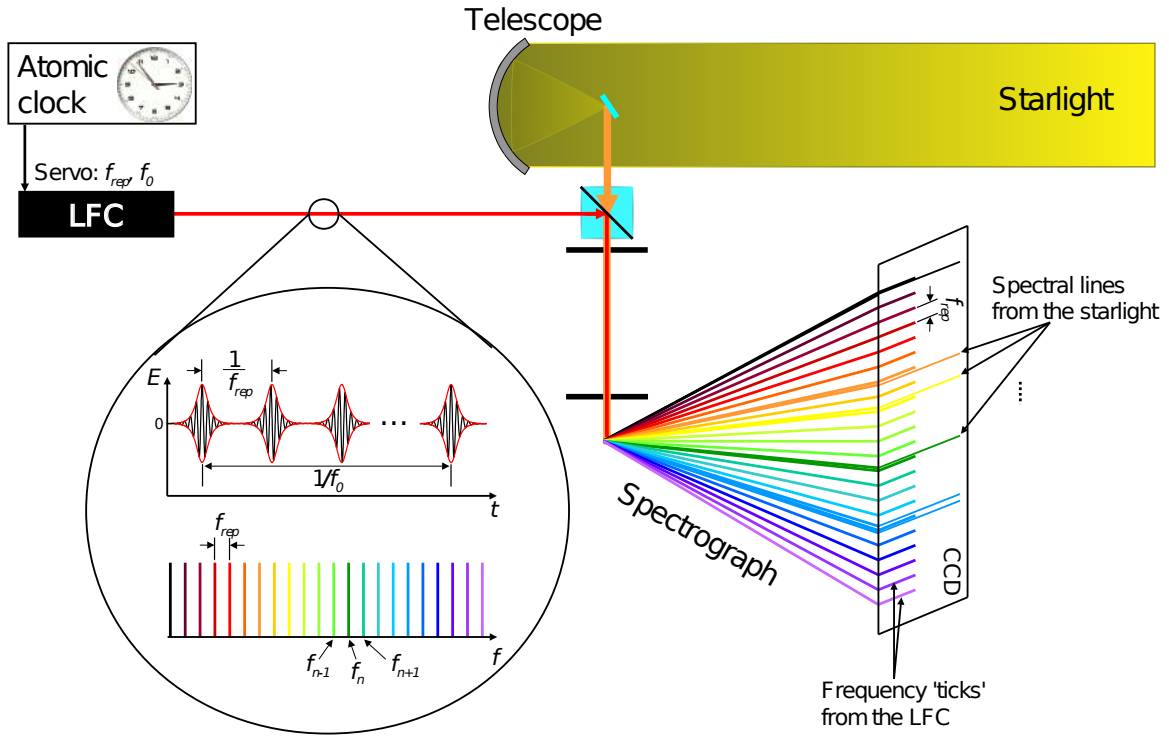


Figure 1.2: Calibration of an astronomical spectrometer using a femtosecond comb. The repetition rate,  $f_r$ , and the carrier envelope offset frequency,  $f_0$ , are first stabilized via a phase lock to an atomic clock. Then the light from the femtosecond comb is superimposed with the light from the telescope. The 'ticks' that appear from this overlap with the stable frequency ruler provided by the femtosecond comb allow for a precise, in-place calibration of the spectrometer. Modified image - original courtesy of Dr. Thomas Schibli.

## Chapter 2

### Noise in Lasers

Like other optical instruments, lasers suffer from various types and sources of noise, some of which can be suppressed via laser design and a judicious choice of materials. The source of all noise in laser systems can generally be divided into two distinct categories: quantum noise, which is primarily related to the spontaneous emission of photons in the laser's gain medium, and technical noise, which is caused by noise originating from the laser's construction and components (i.e. mirror vibrations, pump noise, etc.) [11].

#### 2.1 Types of Noise in Continuous Wave Lasers

The most basic type of laser is the continuous wave laser. This type of laser operates approximately at a single frequency and suffers from a smaller range of noise sources than modelocked laser systems. Both the quantum and technical noise sources in continuous wave lasers can be further divided into two categories: intensity and phase noise.

##### 2.1.1 Intensity Noise

Intensity noise describes the degree of fluctuations in the output power of a laser. Therefore, the use of the term "intensity" is a misnomer in the sense that the intensity noise of a laser is usually described by the r.m.s. (root mean squared) of a laser's output power fluctuations [12]. That is:

$$\delta P_{rms} = \sqrt{\langle (P(t) - \bar{P})^2 \rangle} \quad (2.1)$$

where  $P(t)$  is the instantaneous output power of the laser at time  $t$  and  $\overline{P}$  is the average output power of the laser. Generally, the fluctuations in output power of a laser will vary with frequency, and therefore, it is nearly meaningless to define the quantity in equation 2.1 without first specifying the bandwidth of the instrument used to measure the output power [12]. For this reason, it is more appropriate to define the intensity noise using a power spectral density (PSD) measurement.

#### 2.1.1.1 Aside: Power Spectral Density

A PSD measurement aids in the determination of noise sources (for a specific type of noise, i.e. intensity, phase, etc.) in a given laser by associating a degree of noise power with each frequency measured. The PSD,  $S(f)$ , for a generic, time-varying quantity,  $\chi(t)$ , around a long-term average value (such as instantaneous and average power, respectively, in the case of intensity noise) is determined by equation 2.2 [13].

$$S(f) = \lim_{\tau \rightarrow \infty} \frac{1}{\tau} \langle |\int_{-\frac{\tau}{2}}^{+\frac{\tau}{2}} \chi(t) e^{+i2\pi k} dt|^2 \rangle \quad (2.2)$$

A PSD intensity noise spectrum of a generic solid-state laser is provided as an example for the reader in figure 2.1.

The intensity noise PSD for a laser is usually measured using a photodetector and an electronic spectrum analyzer and is almost always averaged over many measurements. The units for an intensity noise PSD is usually dBc/Hz, which is the magnitude in decibels of the noise relative to the carrier per frequency in hertz.

It should be noted here that there is a potential point of confusion in that the PSD for any signal can be expressed as either one or two sided (also known as a "folded" PSD). For a one-sided PSD, the frequency components of a spectrum are represented only in the positive frequency domain and is relatively intuitive. For a two-sided PSD of a real world signal, the same frequency components are represented on both sides of the carrier with each frequency component having half of the power that it would have in a one-sided PSD, thus

representing the same amount of total power as the latter.

### 2.1.1.2 Relaxation Oscillations

Class B lasers, which include solid state and most diode lasers, exhibit a phenomenon known as relaxation oscillations. These oscillations stem from the fact that in Class B lasers the upper-state lifetime of the gain medium is much longer than the cavity damping time [14], and therefore, are an example of a type of quantum intensity noise. This characteristic is in contrast to class A lasers, such as many gas lasers, which have a cavity damping time which is much longer than the upper-state lifetime of the gas medium and hence exhibit an exponential decay (i.e. over-damped behavior) to the steady state with changes in pump power, rather than a damped oscillation [14]. Therefore, Class B lasers experience under-damped oscillations due to changes in pump power, manifesting as intensity noise in their intensity PSDs, near the relaxation oscillation frequency. It should be noted here that some types of laser can operate

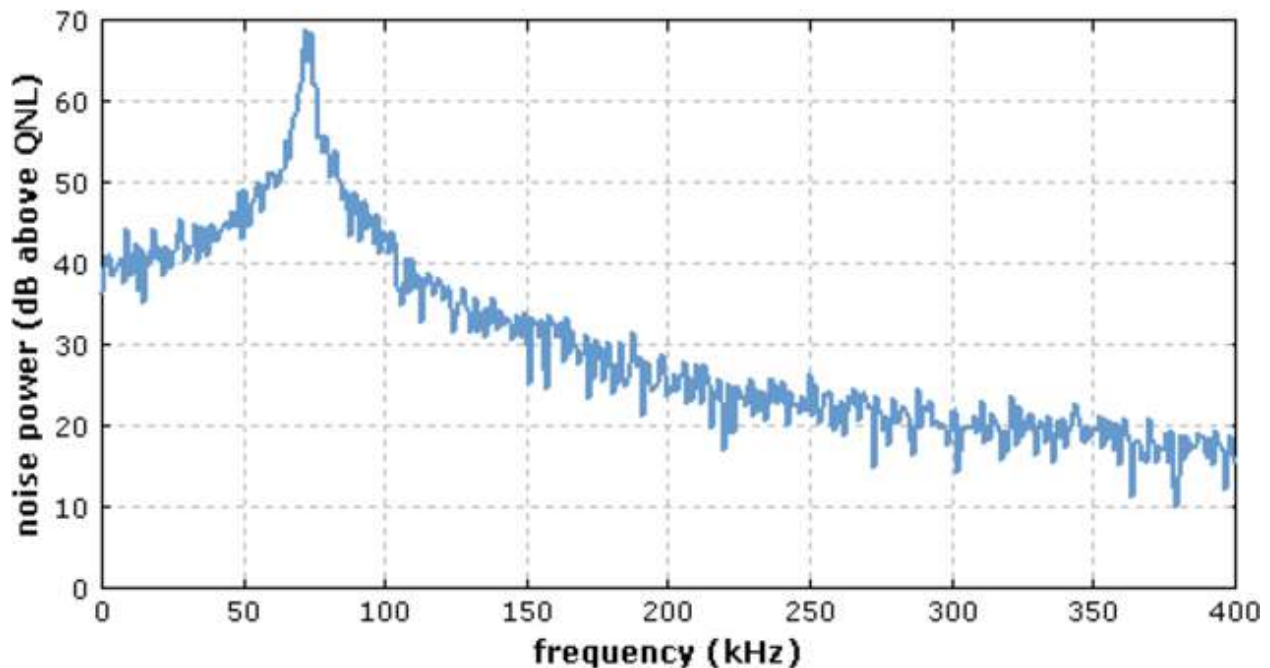


Figure 2.1: A generic solid state laser power spectral density intensity noise spectrum. "QNL" stands for quantum noise limit. Note that the relaxation oscillation frequency,  $f_{ro}$ , is clearly visible at around 70 kHz. Figure used with permission from Dr. Rüdiger Paschotta [13].

in both regimes, depending on the power at which the gain medium is pumped. Where the relaxation oscillation frequency is located for given laser setup is determined by the following formula (assuming small fluctuations and linearization around the steady state) [14]:

$$f_{ro} = \frac{1}{2\pi} \sqrt{\frac{IP_{int}}{T_R E_{sat}} - \frac{1}{4} \left( \frac{1}{\tau_g} + \frac{P_{int}}{E_{sat}} \right)^2} \quad (2.3)$$

where  $P_{int}$  is the lasers' intracavity power,  $I$  is the laser's resonator losses,  $T_R$  is the round-trip time of the laser resonator, and  $E_{sat}$  and  $\tau_g$  are the saturation energy and the upper-state lifetime of the gain medium, respectively. The cavity damping time is then:

$$\tau_{damp} = \frac{T_R}{I} \quad (2.4)$$

As mentioned above, Class B lasers have a short cavity damping time relative to their gain medium's upper-state lifetime, and therefore, the first term in the radical of equation 2.3 dominates and the expression for the relaxation oscillation frequency of Class B lasers reduces to:

$$f_{ro} \approx \frac{1}{2\pi} \sqrt{\frac{IP_{int}}{T_R E_{sat}}} \quad (2.5)$$

Therefore, the frequency of the characteristic peak in most solid-state lasers' intensity PSDs can be approximately determined by the relatively simple equation 2.5. It is important to note that the relaxation oscillation frequency,  $f_{ro}$ , is simply a resonance of the laser setup and that any noise (above the quantum noise limit) that occurs at this frequency must have an origin, such as noise intrinsic to the pump source. An example of an intensity PSD from a generic solid-state laser is shown in figure 2.1.

In addition to the large intensity noise peak caused by relaxation oscillations, small and sharp intensity noise peaks can emerge in the PSD which represent acoustic influences on the laser cavity itself [12]. These acoustic resonances are a primary example of intensity technical noise, as they are directly related to the laser's construction and components, i.e.

not intrinsic to any fundamental properties of the lasing medium or optical phenomena. It is interesting to note that this acoustic noise will also likely increase the phase noise of the laser at the same resonance frequencies.

Lastly, although the intensity noise from quantum sources cannot be eliminated in a given laser system, the effects of this noise can be mitigated with several methods [12]. For example, a pumping diode laser must be of high quality construction and powered by a well-stabilized electrical current source in order to achieve the lowest influence of pump fluctuations on a bulk laser's intensity noise spectrum. Furthermore, cavity parameters, such as total length of the laser resonator, can be adjusted in order to minimize the influence of quantum noise effects [12]. For example, the length of a solid-state laser resonator could be adjusted (thereby changing the round-trip time,  $T_R$ ) according to equation 2.5 to move the relaxation oscillation intensity noise peak to a spectral region which is not of interest for a specific experiment.

### 2.1.2 Phase Noise

In the most basic terms, phase noise quantifies the phase fluctuations of the electric and magnetic field of a laser's optical output. However, this description of phase noise quickly becomes ineffective when lasers with multiple oscillating resonator modes are considered, as is necessary for modelocked lasers and CW lasers with higher-order resonator modes present. Therefore, for the purposes of the immediately following discussion, only CW lasers with all of the power in one resonator mode are considered to better provide the reader with a fundamental description of phase noise. Similarly to intensity noise, phase noise is also generally quantified using a power spectral density (PSD),  $S_\phi(f)$ . It is important to note here that frequency and phase noise PSDs essentially contain the same information and are related by equation 2.6 [15]:

$$S_\nu(f) = f^2 S_\phi(f) \quad (2.6)$$

where  $S_\nu(f)$  is the PSD for frequency noise and  $f$  is the noise frequency.

In the quantum regime, phase noise results mainly from a change in the overall optical phase of a laser's output through the process of *spontaneous emission* [12]. Unlike with stimulated emission, the photons emitted from the gain medium via the process of spontaneous emission are not temporally aligned with the photons already oscillating in the cavity, leading to random phase contributions from this effect in the classical electromagnetic wave picture. These random phase contributions for the output of the laser can cause the phase of the output beam to drift unbounded, as there is a divergence of the phase noise PSD,  $S_\phi(f)$ , at  $f = 0$  (see equation 2.6). This is in contrast to intensity noise, where noise phenomena like oscillation relaxations eventually decay back to a steady state. This inability to set a bound on the drift of the phase noise makes the problem of quantifying this type of noise much more mathematically challenging than for intensity noise. Furthermore, just as with intensity noise, the optical phase of a laser's output can be further altered by changes in system temperature and the acoustic resonances of the laser's components (which, similar to intensity noise, show up as sharp peaks in the phase noise PSD,  $S_\phi(f)$ ).

One of the primary consequences of phase noise in a CW laser is the establishment of a finite value for the linewidth of the laser. That is, phase noise is the fundamental reason why a so-called "single frequency" CW laser still has a non-zero spectral width of its output beam. In fact, even if a CW laser has an ideal design, perfect construction and no mechanical resonances (thereby eliminating any sources of technical noise) the laser will still be affected by the quantum phase noise described above and have a linewidth described (slightly incorrectly) by an equation derived from a linewidth expression for MASERS in 1958 by Schawlow and Townes [16]:

$$\Delta\nu_{out} = \frac{4\pi h\nu(\Delta\nu_{res})^2}{P_{out}} \quad (2.7)$$

where  $\Delta\nu_{out}$  is the *half*-width half-maximum of the linewidth of the laser's output,  $h$  is

Plank's constant,  $\nu$  is the frequency of the single mode oscillating in the laser cavity,  $P_{out}$  is the output power of the laser and  $\Delta\nu_{res}$  is the *half*-width half-maximum of the resonances of the laser resonator. This equation was later refined by Lax in 1967 who showed that a laser's linewidth above threshold must be twice as small, taking Lax's correction into account and adjusting equation 2.7 to describe the linewidth quantities in terms of *full*-width half-maximum yields equation 2.8 [17]:

$$\Delta\nu_{out} = \frac{\pi h\nu(\Delta\nu_{res})^2}{P_{out}} \quad (2.8)$$

Therefore, with an absolute minimum of phase noise in a CW laser, i.e. the phase noise that results from the unavoidable quantum noise limit, the ideal laser still has a finite spectral linewidth of its output.

#### 2.1.2.1 Measurement of Phase Noise

The methods used to measure the phase noise of a laser's output are considerably more complex than the ones used to measure intensity noise. This is because a phase reference is required to measure the phase evolution of a laser's output, preferably a reference which has a lower phase noise than the laser output to be measured. If one has access to a similar laser with a phase noise known to be significantly lower than the laser to be measured, the output of both lasers can be mixed together, producing a low frequency beat note from which the phase noise of the laser of interest can be determined. This technique is conceptually simple, but has the very impractical limitation that an extra, low-noise laser with nearly identical lasing frequencies be available, so that the beat frequency between their outputs is low enough to be precisely measured [12]. Alternatively, a second laser which is nearly identical to the laser whose phase noise is to be measured can be used, but this technique will only be able to provide an estimate for the phase noise characteristics of each laser individually. To avoid the need for a second laser, a phase noise measurement can instead be preformed using a



common technique known as the self-heterodyne method. The self-heterodyne setup (shown in figure 2.2) involves splitting the power of the output beam of the laser to be measured into two equal parts via a beamsplitter. Then, one of these parts is sent through a long delay line (usually a length of optical fiber) while the other part of the beam is sent through an acousto-optic modulator (AOM) to subtly shift the frequency of this beam. Finally, the beams are recombined and shown onto a single photodetector which records the beat note between the delay and frequency-shifted beam. One drawback of this technique is that it requires a very long fiber delay, which is often expensive or impractical. The self-heterodyne method can be preformed with a short delay line (i.e. less than the coherence length of the laser), but then requires relatively complicated mathematics to retrieve the phase, as the long delay line allows for the beams phases' to become uncorrelated [12].

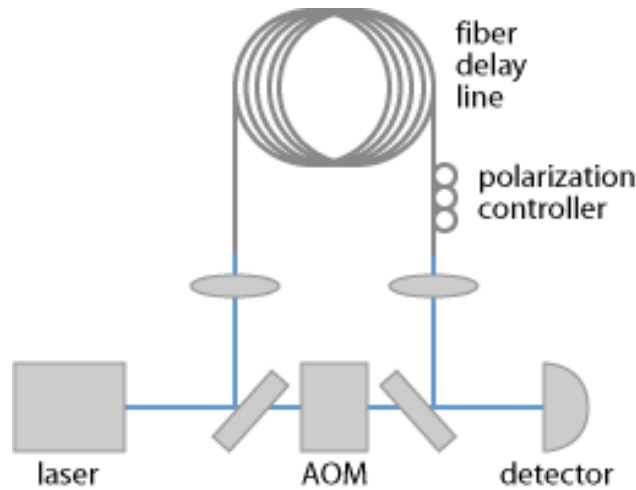


Figure 2.2: An example of a Self-Heterodyne Setup. Figure used with permission from Dr. Rüdiger Paschotta [18].

## 2.2 Noise in Modelocked Lasers

The sources and effects of noise in modelocked laser systems are significantly more complex than those in lasers which operate as continuous wave (CW). The following section will introduce the types and mechanisms of noise in modelocked laser systems, as well as

show how they can be modeled, measured and mitigated.

### 2.2.1 From Waves to Pulses: A Brief Introduction to Passive Modelocking

There exist several prominent types of pulsed lasers, including Q-switched, excimer and gain switched lasers, among others. However, pulsed lasers which are created using a technique known as *passive modelocking* are able to produce the shortest light pulses as of this writing (on the order of femtoseconds with Kerr-lens modelocked Ti:sapphire lasers). The basic idea behind the technique of modelocking is as follows: a fixed phase is introduced (typically by an intracavity device or material) to the many longitudinal modes which oscillate inside of a laser resonator, then, constructive interference between these "phase-locked" modes causes a very temporally short drop in the losses of the laser resonator which leads to a subsequent spike in the optical power output of the modelocked laser, i.e. the emission of a pulse of light (shown in figure 2.3). The fundamental mathematics behind this process are described below.

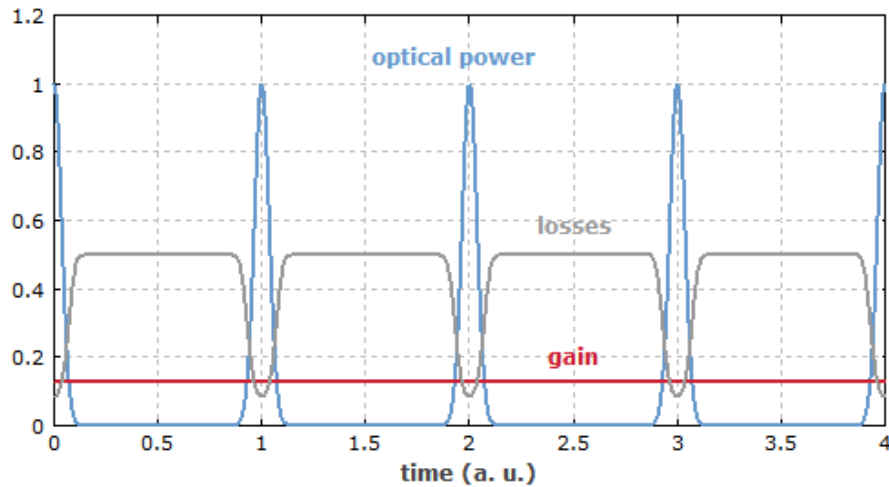


Figure 2.3: Gains, losses and optical power over time in a passively modelocked laser locked with a fast saturable absorber. Note that the gain of the laser is constant, while the saturable absorber, for a short time, reduces the losses below the constant gain of the laser, causing a short pulse of optical power to be emitted. Figure used with permission from Dr. Rüdiger Paschotta [19].

In general, a laser resonator has many modes which are oscillating in the cavity at any given time, according to equation 2.9:

$$L = q \frac{\lambda}{2} \quad (2.9)$$

where  $L$  is the length of the laser cavity,  $\lambda$  is the wavelength of the light oscillating in the cavity and  $q$  is a mode number.

Equation 2.9 demonstrates that there can be many different longitudinal modes oscillating in a laser cavity at any time. For example, with  $L = 300$  mm and  $\lambda = 1550$  nm, the highest allowed mode order is  $q \approx 390,000$ . Furthermore, the spacing in frequency between these longitudinal modes is fixed and described by equation 2.10:

$$\Delta\nu = \frac{c}{2nL} \approx \frac{c}{2L} \quad (2.10)$$

where  $c$  is the speed of light and an air medium ( $n \approx 1$ ) is assumed for the second expression. The quantity  $\Delta\nu$  above is known as the free spectral range (FSR).

In one method of passive modelocking, a device known as a semiconductor saturable absorber mirror (SESAM) is used in place of a normal end mirror inside of the laser cavity. The SESAM gives "preference", or decreased losses, to light of higher intensity. Therefore, after many round trips in the cavity, the longitudinal modes which have the same phase interfere constructively and are "rewarded" by the SESAM with decreased losses. Therefore, after many round trips in the cavity, phase-locked packets of high intensity light will oscillate in the laser resonator, producing a chain of pulses which are partially transmitted through the laser's output coupler mirror. Using the ideas of a Fourier Transform, it can be easily demonstrated that light which is composed of many spectral (frequency) components, or longitudinal modes, leads to shorter pulses in the time domain. This idea is shown graphically in figure 2.4.

Finally, it should be noted that the (ideally) regular chain of pulses produced has a

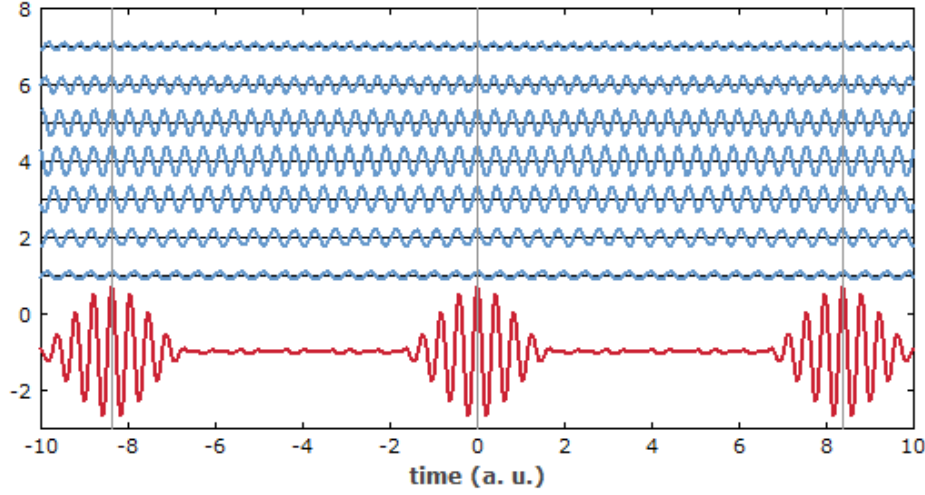


Figure 2.4: Illustration of addition of many longitudinal cavity modes to form a short pulse in the time domain. Due to the properties of Fourier transforms, the more spectral (frequency) components in the pulse, the shorter the pulse will be in the time domain. Figure used with permission from Dr. Rüdiger Paschotta [20].

repetition rate (i.e. pulse frequency) determined by the FSR (equation 2.10) of the laser cavity. That is:

$$f_{rep} = \frac{1}{\tau} = \frac{c}{2L} = \Delta\nu \quad (2.11)$$

where  $f_{rep}$  is the repetition rate of the modelocked laser and  $\tau$  is the time taken for the pulses to make one *round-trip* in the modelocked laser's cavity.

### 2.2.2 Timing Jitter

As mentioned in the previous section, modelocked lasers emit a train of pulses that are equally spaced in the time domain according to equation 2.11. However, noise in the modelocked laser prevents the temporal spacing of these pulses from being exactly constant. The deviation in the time domain spacing of these pulses from the average is characterized by a parameter known as timing jitter (a visual representation of timing jitter is provided in

figure 2.5).

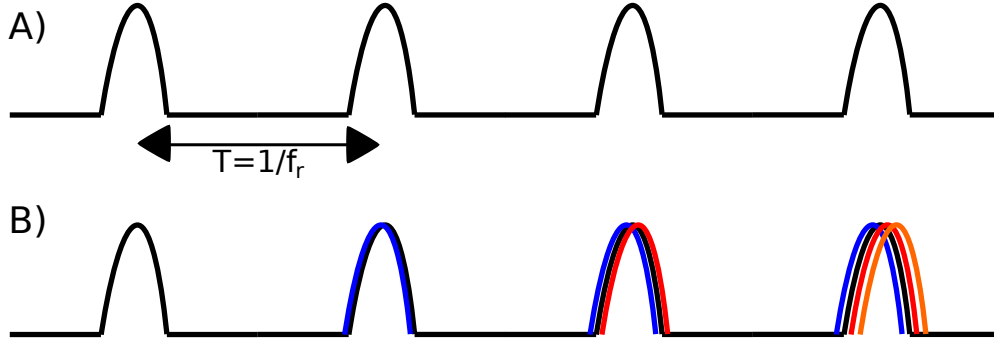


Figure 2.5: A visual representation of timing jitter. Case A) shows a pulse train with zero timing jitter, which is physically unrealistic. Case B) shows a pulse train with many possible degrees of timing jitter.

In general, the timing jitter of a modelocked laser is coupled to a range of other parameters such as intensity noise and pulse duration. Therefore, fully characterizing the timing jitter of a modelocked laser remains a large problem for laser scientists who wish to minimize it via laser design (see section 1.1 for the motivation for the reduction of timing jitter in modelocked lasers). While several influential analytical and numerical methods have been developed, including the famous Haus-Mecozzi analytical model [21], completely describing the coupling of the aforementioned parameters remains a challenge.

### 2.2.2.1 Haus Master Equation

An analytical model of particular prominence was developed by Haus et al. in 1991, as published in their seminal theoretical work, "Structures for additive pulse mode locking" [22]. In this work, Haus et al. present equations of motion for pulse energy, carrier linewidth, frequency pulling (essentially, an effect of the difference between allowed longitudinal modes when a lasing medium has a population inversion vs is turned off) and timing jitter. A slightly modified version of Haus' "Master Equation" from a 1993 paper, which describes the

nonlinear pulse evolution for given cavity parameters, is presented below [21]:

$$T_R \frac{\partial}{\partial T} a = \left[ -l + g \left( 1 - \frac{1}{\Omega_g} \frac{\partial}{\partial t} + \frac{1}{\Omega_g^2} \frac{\partial^2}{\partial t^2} \right) + jD \frac{\partial^2}{\partial t^2} + (\gamma - j\delta) |a|^2 \right] a + T_R S(t, T) \quad (2.12)$$

where  $T$  is the "slow time" variable (time evolution over many round trips),  $t$  is the short-time variable,  $T_R$  is the round-trip time,  $a(T, t)$  is the electrical field amplitude inside of the laser cavity,  $l$  and  $g$  are the incremental loss and gain, respectively,  $\Omega_g$  is the gain bandwidth,  $\gamma$  is the effective saturable absorber action,  $\delta$  is the Kerr phase modulation coefficient,  $D$  is the group velocity dispersion coefficient, and  $S(t, T)$  is the time-dependent noise source.

#### 2.2.2.2 Numerical Model: Timing Jitter Characterization

As equation 2.12 clearly demonstrates, when one considers the solution of the intracavity electric field,  $a(T, t)$  for every type of possible noise, the analytical characterization of a modelocked laser's properties becomes quite complex. Therefore, it is often desirable to work with *numerical* rather than analytical methods. One such method that has gained significant popularity was introduced by Rüdger Paschotta in his 2004 paper entitled "Noise of mode-locked lasers (Part I): numerical model" [2]. Paschotta's numerical model agrees with the Haus-Mecozzi analytical model [2] and provides a more straightforward approach to characterizing the types and degree of noise in a modelocked laser. First, Paschotta assumes that all pulses in the output of such a laser are entirely separable, which is usually a very reasonable assumption. Then, the temporal position of a pulse is defined by the following [2]:

$$t_p \equiv \frac{\int t P(t) dt}{\int P(t) dt} \quad (2.13)$$

where  $P(t)$  is the instantaneous optical power at time  $t$ .

Then, a timing error is defined, which is the temporal deviation of a single pulse from the corresponding pulse position of a theoretical modelocked laser with no noise. This timing

error is more practical in terms of a phase error,  $\Delta\phi$  [2]:

$$\Delta\phi = 2\pi f_{rep}\Delta t \quad (2.14)$$

where  $f_{rep}$  is the repetition rate and  $\Delta t$  is the aforementioned timing error. Note that equation 2.14 is the phase noise of the lowest harmonic in a detected pulse train, not the phase noise of the optical pulses themselves. Therefore, Paschotta refers to this noise as "timing phase noise". Furthermore, Paschotta defines the timing phase power spectral density,  $S_\phi(f)$ , as [2]:

$$S_\phi(f) \equiv \lim_{T \rightarrow \infty} \frac{1}{T} \left| \int_{-\frac{T}{2}}^{\frac{T}{2}} \Delta\phi(t) e^{+i2\pi ft} dt \right|^2 \quad (2.15)$$

where the limit  $T \rightarrow \infty$  is introduced outside of the squared modulus of the Fourier transform to prevent divergence. Note: Here,  $S_\phi(f)$  is defined as a two-sided PSD, such that  $\mathcal{L} \equiv S_\phi(f)$ .

This timing phase PSD can then be related to the PSD of the instantaneous repetition frequency by equation 2.16 [2]:

$$S_\phi(f) = \frac{1}{f^2} S_{f_{rep}}(f) \quad (2.16)$$

where  $S_{f_{rep}}(f)$  is the instantaneous repetition frequency PSD and  $f$  is the noise frequency.

Furthermore, for the timing noise PSD,  $S_{\Delta t}(f)$  [2]:

$$S_{\Delta t}(f) = \left( \frac{\bar{T}}{2\pi} \right)^2 S_\phi(f) = \left( \frac{1}{2\pi f_{rep}} \right)^2 S_\phi(f) \quad (2.17)$$

where  $\bar{T}$  is the mean period between pulses (i.e.  $\bar{T} = \frac{1}{f_{rep}}$ ).

When only quantum noise sources are considered, that is, for a hypothetical laser with no technical noise, the following expression for the timing noise PSD is obtained [23]:

$$S_{\Delta t}(f) = \frac{1}{(2\pi f)^2} \frac{h\nu}{E_p^2} \frac{2g}{T_R} \int t^2 P(t) dt \quad (2.18)$$

where  $h\nu$  is the photon energy,  $E_p$  is the energy of a single pulse,  $T_R$  is the round-trip time of the pulse and  $g$  is the intensity gain.

Another effect of interest in fully characterizing the noise of a modelocked laser is the change of cavity length via the vibration of the resonator mirrors. This effect is handled by Paschotta's numerical model in the following manner. The accumulated timing error for these mirror vibrations is [23]:

$$\Delta t(t) = \frac{1}{T_{rt}} \int_0^t \delta T_{rt} \sin(2\pi f t') dt' = -\frac{1}{T_{rt}} \delta T_{rt} \frac{\cos(2\pi f t)}{2\pi f} \quad (2.19)$$

where a sinusoidal oscillation of the round-trip time,  $T_{rt}$ , with the small amplitude  $\delta T_{rt}$  at the frequency,  $f$ , is assumed. The dependence on  $\frac{1}{T_{rt}}$  demonstrates that a resonator with a short cavity length (i.e. a short round-trip time) will have an increased timing error contribution from the vibration of the cavity mirrors. Equation 2.19 also describes the effective change in cavity length that occurs from fluctuations in the index of refraction of the gain medium, i.e. from thermal effects [23]. Equation 2.19 can then be generalized to a power spectral density,  $S_{T_{rt}}(f)$ , which leads to a contribution to the timing noise PSD,  $S_{\Delta t}(f)$  of [23]:

$$\Delta S_{\Delta t}(f) = \left( \frac{1}{2\pi f T_{rt}} \right)^2 S_{T_{rt}}(f) \quad (2.20)$$

which can then be added to the other contributions to the timing noise.

In addition to the effects in this section, center frequency shifts, pulse duration noise and intensity noise, are in general, coupled to the timing jitter of a modelocked laser.

### 2.2.2.3 Center Frequency Shifts

Like their continuous wave counterparts, modelocked lasers are subject to shifts in their center frequency. As in CW lasers, this is primarily due to the spontaneous emission from the gain medium, which introduces photons with a random phase. In a modelocked laser, this leads to a corresponding random shift in the pulse position, but also changes in the group velocity with dispersion in the cavity. These changes in group velocity lead directly to a fluctuation in pulse timing, thus contributing to the overall timing jitter of the pulses [2].



This effect is known as Haus-Gordon timing jitter. It is notable that Haus and Mecozzi in [21] identified these effects, but did not realize that they have no dependence on a soliton pulse-shaping mechanism [2].

#### 2.2.2.4 Pulse Duration Noise

In the Haus-Mecozzi analytical model of noise in modelocked lasers [21], pulse duration is not considered an independent dynamical variable, and therefore, the model is unequipped to describe the coupling of pulse duration noise to timing jitter. However, for a fast saturable absorber, fluctuations in pulse duration are *not* coupled to timing jitter. On the other hand, for slow saturable absorbers, there exists a coupling between pulse duration and timing jitter as the absorber shifts the intracavity pulses in the time domain by a quantity proportional to the pulse duration [23]. Furthermore, in general, pulse duration and energy are coupled to each other and so can both contribute to timing jitter.

Despite having no appreciable effect on the timing jitter of pulses from a modelocked laser with a fast saturable absorber, pulse duration can exhibit a coupling with the intensity noise of these types of lasers. This is because changes in pulse duration result in fluctuations in the peak power of the intracavity pulses and thus modify the losses at the fast saturable absorber [23].

#### 2.2.2.5 Intensity Noise

Timing jitter can also couple to the intensity noise of modelocked lasers. Although the coupling is far more pronounced in modelocked lasers with slow saturable absorbers, those with fast saturable absorbers can also exhibit the coupling under certain circumstances.

For a slow saturable absorber, the leading part of an intracavity pulse is attenuated more than the trailing part, which leads to a shift in the time domain of the pulse. This in turn leads to the equivalent of a slight increase of cavity length, which causes a decrease in the repetition rate of the laser. In fact, this effect bounds the noise amplification in the

circulating pulses, allowing for very slow saturable absorbers (i.e. with recovery times more than a factor of ten as long as the pulse duration) to create stable trains of pulses [23]. However, because the magnitude of the temporal shift of the intracavity pulses introduced by a slow absorber depends on the pulse energy, the intensity noise couples to the timing noise as described by equation 2.21 [23]:

$$\Delta S_{\Delta t}(f) = \left( \frac{1}{2\pi f T_{rt}} \frac{\partial \Delta t}{\partial s} s \right)^2 S_I(f) \quad (2.21)$$

where  $\Delta t$  is the timing error caused by the intensity noise,  $S_I(f)$ , and  $s$  is the saturation parameter defined as the ratio of intracavity pulse energy and the saturation energy of the saturable absorber.

Furthermore, for the timing phase noise [23]:

$$\Delta S_{\phi}(f) = (2\pi f_{rep})^2 \Delta S_{\Delta t}(f) = \left( \frac{f_{rep}^2}{f T_{rt}} \frac{\partial \Delta t}{\partial s} s \right)^2 S_I(f) \quad (2.22)$$

Note that if the slow saturable absorber is operated where the maximum temporal shift occurs, then:

$$\frac{\partial \Delta t}{\partial s} = 0 \quad (2.23)$$

Then, the right-hand side of equations 2.21 and 2.22 would vanish, indicating that the coupling between timing and intensity noise would be eliminated.

### 2.3 Beam Pointing Fluctuations

It should be briefly discussed here that both continuous wave and modelocked lasers can suffer from a group of phenomena known as beam pointing fluctuations. Beam pointing fluctuations are a type of noise that change the position of a beam's focus, or more generally, a laser cavity's modes [24]. Keeping the position of a beam's focus stable is important for many applications, including the coupling of light into a cavity. In particular, vibration of cavity

mirrors and other optical components can lead to a shifting of the beam focus. However, thermal effects within a laser's gain medium can also lead to beam pointing fluctuations which are dependent on changes in pump power - the degree of which is strongly dependent on the quality of alignment of the pump beam and laser resonator [24]. Lastly, all of these effects can be modeled as dynamically changing misalignments, helping to pinpoint the source of beam pointing fluctuations.

## 2.4 Noise in Lasers vs Passive Reference Cavities

One of the fundamental requirements of most types of laser stabilization techniques is an oscillator, or other type of reference, which is significantly less noisy than the laser to be stabilized. For this reason, optical reference cavities are often produced with materials which have very low thermal expansion coefficients, such as quartz. By producing reference cavities from these types of materials, the cavity length can be stabilized, and therefore, the round-trip time of light oscillating in the cavity will remain very constant. For example, if one uses for an optical frequency reference a 100 mm cavity made from pure silicon (linear thermal expansion coefficient:  $\alpha_L \approx 3 \frac{10^{-6}}{\text{K}}$  [25]) then a change of 1 degree Kelvin of the cavity will lead to a change in length of approximately:

$$\Delta L \approx \alpha_L \Delta T L = \left( 3 \frac{10^{-6}}{\text{K}} \right) (1 \text{ K})(0.1 \text{ m}) = 3 \times 10^{-7} \text{ m} \quad (2.24)$$

A change of 0.0003% due to the change in the temperature of the silicon.

If 1550 nm light was traveling in this cavity, this thermal change would correspond to a shift in optical frequency,  $\delta\nu$ , of:

$$\delta\nu = \frac{\Delta L}{L} \nu = \left( \frac{3 \times 10^{-7} \text{ m}}{0.1 \text{ m}} \right) (1.934 \times 10^{14} \text{ Hz}) = 5.802 \times 10^8 \text{ Hz} \approx 580 \text{ MHz} \quad (2.25)$$

Thus, the use of materials with very low thermal expansion coefficients to build reference cavities allows for a very temperature-stable frequency discriminator. Of course, thermal

expansion is not the only noise that reference cavities are subjected to. For example, even with perfect construction, the Brownian motion of the dielectric mirror coatings still add noise to the reference cavity.

In comparison to the reference cavities described above, laser resonators are subjected to far greater range of types and magnitude of noise sources. For example, laser resonators suffer from amplified spontaneous emission (ASE), pump noise, relaxation oscillation noise and nonlinearities in gain mediums, to name a few significant sources of noise that reference cavities do not experience. However, the largest advantage that passive cavities have over lasers as references is the ability to achieve a very high finesse.

#### 2.4.1 Cavity Finesse

Finesse is related to the quality factor (alternatively Q-factor) commonly used in electronics and helps describe the "sharpness" of a cavity's resonances. Finesse can also be thought of as a measurement of a cavity's optical loss and is defined by the following equivalent equations[26]:

$$\mathcal{F} = \frac{FSR}{FWHM} = \frac{\frac{c}{2nL}}{\Delta\nu_{\frac{1}{2}}} = \frac{\pi(r_1 r_2)^{\frac{1}{4}}}{1 - (r_1 r_2)^{\frac{1}{2}}} \quad (2.26)$$

where  $\mathcal{F}$  is the cavity finesse,  $FSR$  is the free spectral range,  $FWHM$  and  $\Delta\nu_{\frac{1}{2}}$  are the full spectral width at half-maximum,  $n$  is the index of refraction,  $L$  is the length of the cavity and  $r_1$  and  $r_2$  are the reflectivity of the first and second mirror of a two-mirror cavity, respectively.

Furthermore, the quality factor,  $Q$ , can be related to the finesse via the following [27]:

$$Q = \frac{nL}{\lambda} \mathcal{F} = \frac{\nu_0}{\Delta\nu_{\frac{1}{2}}} \quad (2.27)$$

where  $\lambda$  is the wavelength of light oscillating in the cavity,  $\nu_0$  is the resonance frequency and  $\Delta\nu_{\frac{1}{2}}$  is the full spectral width (i.e. bandwidth) of the optical resonator at half-maximum.

Alternatively, for an optical cavity, one can think of  $Q$  as the ratio of the energy stored

in the cavity at resonance to the energy lost in an oscillation cycle (times  $2\pi$ ) [26].

As can be plainly seen from equations 2.26 and 2.27, a cavity with a high finesse, i.e. low-loss, is able to provide a narrow bandwidth of optical frequencies that will oscillate inside of the cavity. In laser resonators, the finesse is limited due to the fact that lasers must have at least one mirror which is used as an output for the light oscillating in the cavity, that is the output coupler. Furthermore, losses in a laser cavity must be chosen to prevent the build-up of a dangerous amount of optical power that could, in the worst case, destroy either the gain medium or even the pump laser. Therefore, passive cavities have a distinct advantage as optical references over lasers, in that their finesse can be optimized and, theoretically, increased almost without limit.

#### 2.4.2 Passive Optical Cavity Resonances

For light to oscillate in a certain optical cavity of length,  $L$ , the round-trip phase of said light be equal to  $2\pi$  radians. For the Hermite-Gaussian modes, the phase shift,  $\Delta\phi$  of a  $TEM_{m,p}$  mode propagating from  $z = 0$  to  $z = L$  is [26]:

$$\Delta\phi = kL - (1 + m + p) \tan^{-1} \left( \frac{L}{z_0} \right) \quad (2.28)$$

where  $m$  and  $p$  are integers representing the Hermite-Gaussian mode parameters which determine the beam's spatial profile in the x and y directions (i.e. transverse modes), respectively,  $k$  is the wavenumber and  $z_0$  is the position of the beam focus within the cavity.

The phase shift in equation 2.28 leads to the following resonance condition [26]:

$$kL - (1 + m + p) \tan^{-1} \left( \frac{L}{z_0} \right) = q\pi \quad (2.29)$$

where  $q$  is the longitudinal mode number corresponding to the fundamental spacing.

The phase condition in equation 2.29 imposed on the light resonating in a passive cavity

leads to the following Hermite-Gaussian resonance frequencies,  $\nu_{m,p,q}$  [26]:

$$\nu_{m,p,q} = \frac{c}{2nL} \left[ q + \frac{1+m+p}{\pi} \cos^{-1}(g_1 g_2)^{\frac{1}{2}} \right] \quad (2.30)$$

where  $R_{1,2}$  are the radii of curvature for the two mirrors of the cavity and  $g_{1,2} = \left(1 - \frac{L}{R_{1,2}}\right)$  is known as the *stability parameter*.

For the purposes of explanation, let the assumption be made that  $g_1 = g_2 = \frac{1}{2}$ , thus, equation 2.30 reduces to:

$$\nu_{m,p,q} = \frac{c}{2nL} \left( q + \frac{1+m+p}{3} \right) \quad (2.31)$$

From equation 2.31, it can be seen that the separation of the fundamental, longitudinal modes is  $\frac{c}{2nL}$ , the free-spectral range, as expected. However, equation 2.31 also illustrates the fact that multiple values of the transverse mode parameters,  $m$  and  $p$  can correspond to the same resonance frequency, a phenomenon known as *mode degeneracy*. Therefore, it is generally desirable when using a passive optical cavity as a frequency reference to ensure that the transverse mode-matching is correct, such that the effect of mode degeneracy does not overlap the fundamental longitudinal mode with a higher-order transverse mode. For example, note that in equation 2.31 for a symmetric cavity, if the lowest order transverse mode ( $TEM_{0,0}$ ) is coupled into the cavity (as is usually done for frequency discrimination), then the resonances,  $\nu_{1,1,q}$ , correspond exactly to only multiples of the free spectral range,  $\frac{c}{2nL}$ , which ensures a desirable separation of the modes allowed to oscillate in the cavity.

## Chapter 3

### PDH-Based Repetition Rate Stabilization Technique

#### 3.1 Theory: Early Laser Stabilization Techniques

The development of the laser in 1960 began to allow researchers across a range of diverse fields the unprecedented ability to utilize the narrow spectrum of light provided by continuous-wave (CW) lasers in various types of experiments, such as those developed for gravitational wave detection [28]. The success of early experiments performed with lasers would, over the following several decades, lead to a huge demand for more reliable, less costly and higher performance CW lasers. To improve the operation of existing laser systems, the optics community began searching for ways to reduce frequency drift and phase noise - thereby narrowing the spectral linewidth (see section 2.1.2) - of CW lasers. Although the use of passive optical cavities to stabilize the frequency of CW gas lasers dates back to the mid-sixties [29], these techniques generally relied on using the transmitted light through the stabilization cavity to provide feedback (via an electronic servo filter) to the laser cavity's length. However, these techniques suffer from either coupling between intensity and frequency noise or a reduction in stability by using a "side-fringe" lock, where the cavity transmission is adjusted to be near its half-maximum, thus necessitating a reliance on perfectly-matched photodetectors [28]. Furthermore, the "side-fringe" technique suffers from response errors as a consequence of laser intensity instabilities which make it futile to utilize a servo filter bandwidth much larger than the stabilization cavity's linewidth, hence limiting the noise suppression bandwidth of the feedback loop and/or the maximum slope of the discriminator

signal [28].

### 3.1.1 The Pound, Drever, Hall (PDH) Technique

In 1983, Drever et al. published a new phase and frequency stabilization technique [28] which would quickly become the state of the art for creating laser systems with narrow spectral linewidths, known today as the Pound, Drever, Hall (PDH) technique. The primary advantage of this stabilization technique over its predecessors is its complete decoupling of the intensity and phase noise of a laser's output via the use of the *reflected*, rather than transmitted, light from a passive optical cavity. Furthermore, through the introduction of phase modulation to produce sidebands around the carrier, the PDH technique is able to lock when the transmission of the passive optical cavity is at a maximum, thereby circumventing the aforementioned transient response problems [28].

#### 3.1.1.1 PDH Setup

The PDH experimental setup (shown in figure 3.1) consists of a CW laser to be stabilized, whose beam is first propagated through an electro-optic phase modulator, so that the phase of the beam is modulated by a local oscillator's periodic signal (typically a simple sine wave).

Then, the beam is passed through a polarizing beamsplitter, and subsequently, a quarter wave plate - giving the incident light a circular polarization - before reaching the first cavity mirror. If monochromatic light from the CW laser and a lossless Fabry-Perot cavity are assumed, the reflection coefficient,  $F(\omega)$  for the beam incident on the first cavity mirror is [30]:

$$F(\omega) = \frac{E_{ref}}{E_{inc}} = \frac{r \left( \exp\left(i \frac{\omega}{\Delta\nu_{FSR}}\right) - 1 \right)}{1 - r^2 \exp\left(i \frac{\omega}{\Delta\nu_{FSR}}\right)} \quad (3.1)$$

where  $E_{inc} = E_0 e^{i\omega t}$  and  $E_{ref} = E_1 e^{i\omega t}$  are the complex electric fields of the incident and



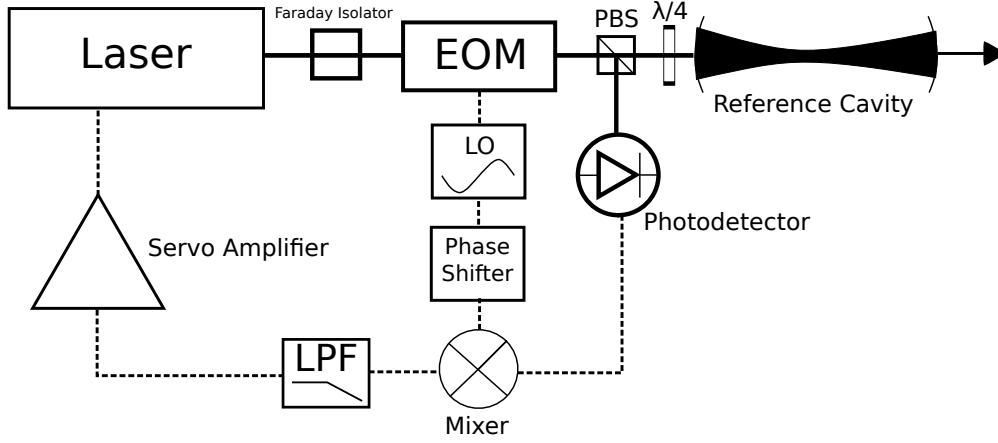


Figure 3.1: A basic outline of the Pound, Drever, Hall (PDH) stabilization setup. Solid lines represent the beam's path, whereas dotted lines represent electronic connections.

reflected beams, respectively,  $\omega$  is the angular frequency of light from the CW laser,  $\Delta\nu_{FSR}$  is the free spectral range and  $r$  is the reflectivity of the mirrors used to construct the passive cavity.

At this point, if the beam is on-resonance with the passive cavity then a portion of the beam's power (specifically the fraction transmitted is  $T(\omega) = 1 - F(\omega)$ ) will couple into the cavity and begin oscillating between the two mirrors that form the cavity. The light reflected from the first cavity mirror will travel through the quarter wave plate again, rotating the polarization such that it is linear again and rotated  $90^\circ$  relative to the incident light. This polarization rotation causes the polarizing beamsplitter to reflect, rather than transmit, this light towards a photodetector (figure 3.1). The stored light energy will then leak from the cavity at both mirrors at a rate determined by the reflectivity of the cavity mirrors and the magnitude of energy stored in the cavity. Referring to section 2.4.1, the Q-factor (or, nearly equivalently, the Finesse, see equation 2.27) determines the leakage rate of the cavity. Therefore, the beam reflected from the first mirror is composed of two components: the beam which has just been reflected from the cavity and a leakage beam from inside of the cavity. Exactly on resonance, the leakage beam and the promptly reflected beam have the same frequency and nearly the same intensity, but the promptly reflected beam is exactly

180° out-of-phase with the leakage beam. This leads to destructive interference where both reflected beams disappear and the light simply transmits through the second mirror of the cavity. If the laser's frequency is instead *near* the resonance of the cavity, a standing wave is still built up in the cavity and the intensity of the leakage beam will still be about the same as the reflected beam, however the two beams will no longer be *exactly* 180° out-of-phase. Therefore, the promptly reflected beam and the leakage beam will not cancel each other out completely and a finite amount of light will be reflected off of the first mirror of the cavity. The phase of this reflected light can be used to determine which side of the cavity resonance the CW laser is on, as illustrated in figure 3.2.

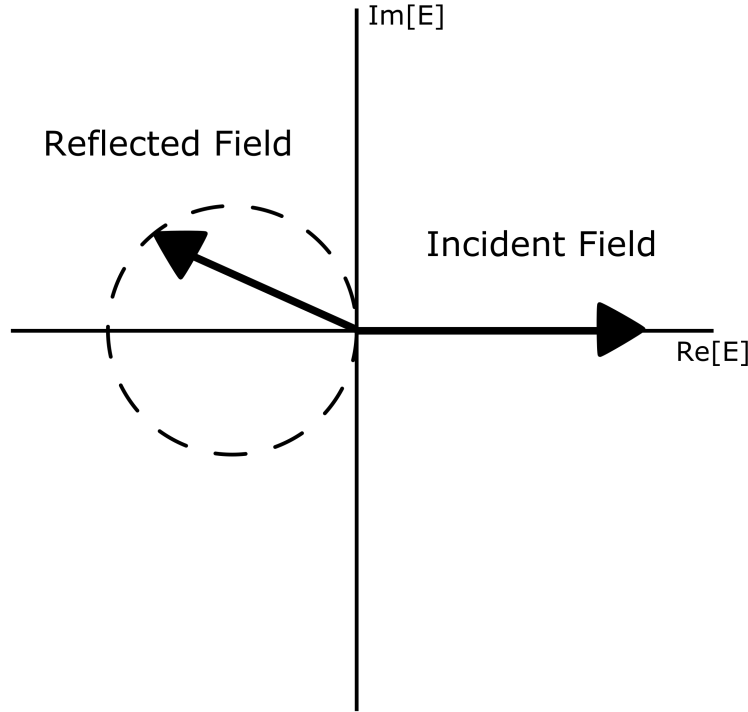


Figure 3.2: A plot of the reflection coefficient,  $F(\omega)$ , from a Fabry-Perot cavity in the complex plane. Note that the imaginary part of the reflection coefficient is in the lower-half plane below resonance and in the upper-half plane above resonance.

As there is no way to directly measure the phase of light reflected from the cavity, the PDH scheme endeavors to indirectly measure the phase by phase-modulating the beam from the CW laser with the aforementioned Pockels Cell, which adds sidebands to the beam.

These sidebands are created by a local oscillator driven at a frequency which will keep them far away from the cavity's bandwidth and provide a fixed phase relationship between the incident and reflected beams from the reference cavity. That is, the sidebands will interfere with the reflected beam and, if the result is demodulated at the sideband frequency, then a beat pattern will be left which reveals the difference in phase between the leakage and reflected beams. This beat pattern is the basis for creating the PDH error signal, as the beat note will become zero when the leakage and reflected beams are exactly in-phase - indicating that the incident beam is exactly on-resonance with the reference cavity (i.e.  $\omega_{laser} = \omega_{cavity}$ ).

### 3.1.1.2 PDH Error Signal

After the output beam of the CW laser to be stabilized passes through the electro-optic phase modulator (figure 3.1) the incident electric field becomes [30]:

$$\begin{aligned} E_{inc} &= E_0 e^{i(\omega t + \beta \sin(\Omega t))} \approx [J_0(\beta) + 2iJ_1(\beta) \sin(\Omega t)] e^{i\omega t} \\ &= E_0 [J_0(\beta) e^{i\omega t} + J_1(\beta) e^{i(\omega + \Omega)t} - J_1(\beta) e^{i(\omega - \Omega)t}] \end{aligned} \quad (3.2)$$

where  $\beta$  is the modulation depth,  $\Omega$  is the phase modulation frequency and  $J_0$  and  $J_1$  are Bessel functions of the first kind. The last form in equation 3.2 is elucidating in that after the phase modulation of the beam by the electro-optic phase modulator, there are now, effectively, three separate beams incident on the cavity: the carrier (with frequency  $\omega$ ) and the sidebands (with frequencies  $\omega \pm \Omega$ ). Furthermore,  $P_0 \equiv |E_0|^2$ , so when the modulation depth is small, i.e.  $\beta < 1$ , the lion's share of the power is present in the carrier and the first order sidebands:  $P_c + 2P_s \approx P_0$ . Then, for the reflected electric field in the PDH setup [30]:

$$E_{ref} = E_0 [F(\omega) J_0(\beta) e^{i\omega t} + F(\omega + \Omega) J_1(\beta) e^{i(\omega + \Omega)t} - F(\omega - \Omega) J_1(\beta) e^{i(\omega - \Omega)t}] \quad (3.3)$$

However, when the reflected beam is picked up by the photodetector (figure 3.1) it is the power that is actually measured, therefore [30]:

$$\begin{aligned}
P_{refl} = |E_{refl}|^2 = & P_c |F(\omega)|^2 + P_s [|F(\omega + \Omega)|^2 + |F(\omega - \Omega)|^2] \\
& + 2\sqrt{P_c P_s} \left[ \text{Re}\{F(\omega)F^*(\omega + \Omega) - F^*(\omega)F(\omega - \Omega)\} \cos(\Omega t) \right. \\
& \left. + \text{Im}\{F(\omega)F^*(\omega + \Omega) - F^*(\omega)F(\omega - \Omega)\} \sin(\Omega t) \right] + (2\Omega \text{ terms})
\end{aligned} \tag{3.4}$$

where  $(2\Omega \text{ terms})$  result from the sidebands interfering with each other.

The terms of interest in equation 3.4 are the ones which oscillate at frequency  $\Omega$ , as they result from the interference of the carrier with the sidebands. It can be shown that at low modulation frequencies, i.e.  $\Omega \ll \frac{\Delta\nu_{FSR}}{\mathcal{F}}$ , then the internal field of the cavity has time to respond and  $F(\omega)F^*(\omega + \Omega) - F^*(\omega)F(\omega - \Omega)$  becomes purely real, thus only the cosine term contributes. Conversely, at high modulation frequencies, i.e.  $\Omega \gg \frac{\Delta\nu_{FSR}}{\mathcal{F}}$ , near resonance,  $F(\omega)F^*(\omega + \Omega) - F^*(\omega)F(\omega - \Omega)$  is purely imaginary, thus only the sine term contributes [30]. Generally, it is desirable to use a high modulation frequency for reasons that will soon be made clear. Therefore, to obtain the phase information required to create an error signal, the signal from the photodetector (equation 3.4) is fed into a RF mixer along with a  $90^\circ$  phase-shifted version of the local oscillator signal used to phase modulate the signal initially (figure 3.1). The output of the mixer is then sent through a low-pass filter, in order to remove the frequency sum and leave the frequency difference (near DC) term. If  $\Omega$  and  $\Omega'$  are the (high modulation frequency) inputs to the mixer, this process is described mathematically by the following equation:

$$\begin{aligned}
\sin(\Omega t) \sin(\Omega' t + 90^\circ) = \sin(\Omega t) \cos(\Omega' t) &= \frac{1}{2} [\sin((\Omega - \Omega')t) - \sin((\Omega + \Omega')t)] \\
&\xrightarrow{LPF} \frac{1}{2} \sin((\Omega - \Omega')t)
\end{aligned} \tag{3.5}$$

Therefore, when  $\Omega = \Omega'$ , the CW laser is exactly on resonance with the passive optical cavity and the DC signal becomes zero. Note: in practice, achieving the  $90^\circ$  phase shift is generally done empirically, due to delays in electrical connections which are difficult to

fully characterize. Thus, the phase of the local oscillator signal is manually adjusted by a phase-shifter until a correct error signal appears (i.e. looks like figure 3.3).

When the carrier is close to the resonance of the reference cavity and the sidebands are created with a fast phase modulation frequency, the sidebands of the incoming beam are completely reflected, as they are well-outside of the reference cavity's acceptance bandwidth. Therefore,  $F(\omega)F^*(\omega + \Omega) - F^*(\omega)F(\omega - \Omega) \approx -i2 \text{Im}\{F(\omega)\}$ , and will be purely imaginary [30]. Then, the PDH error signal,  $\epsilon$ , becomes [30]:

$$\epsilon = -2\sqrt{P_c P_s} \text{Im}\{F(\omega)F^*(\omega + \Omega) - F^*(\omega)F(\omega - \Omega)\} \quad (3.6)$$

which is plotted in figure 3.3.

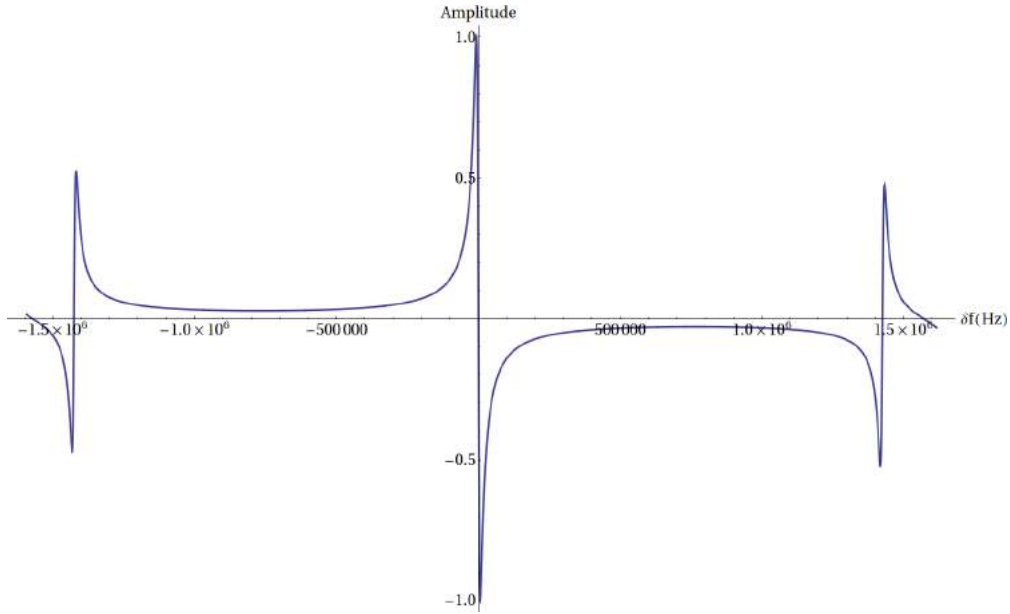


Figure 3.3: A plot of the normalized PDH error signal as a function of spectral distance from resonance,  $\delta f$ , for  $\Omega = 8$  MHz, a free-spectral range of 500 MHz and a mirror reflectivity of 99.3%. The two outlying curves are from the interaction of the carrier with the sidebands. Note that the error signal is asymmetric around resonance, allowing the feedback loop to determine which side of resonance the CW laser is on.

Then the power reflected can be approximated as [30]:

$$P_{ref} = 2P_s - 4\sqrt{P_c P_s} \text{Im}\{F(\omega)\} \sin(\Omega t) + (2\Omega \text{terms}) \quad (3.7)$$

Furthermore, near resonance [30]:

$$\frac{\omega}{\Delta\nu_{FSR}} = 2\pi N + \frac{\delta\omega}{\Delta\nu_{FSR}} \quad (3.8)$$

where  $N$  is an integer and  $\delta\omega$  is the degree of deviance of the CW laser from the reference cavity's resonance.

If it is assumed that the finesse of the reference cavity is large, the reflection coefficient can be written as [30]:

$$F \approx \frac{i}{\pi} \frac{\delta\omega}{\Delta\nu} \quad (3.9)$$

where  $\Delta\nu \equiv \frac{\Delta\nu_{FSR}}{\mathcal{F}}$  is the linewidth of the reference cavity. Equation 3.9 demonstrates that, near resonance, the reflection coefficient is linear in the deviation of the CW laser from resonance,  $\delta\omega$ . This leads to an error signal near resonance described by [30]:

$$\epsilon \approx -\frac{4}{\pi} \sqrt{P_c P_s} \frac{\delta\omega}{\Delta\nu} \quad (3.10)$$

This linear relationship can then be re-arranged as follows:

$$\epsilon \approx -\frac{8\sqrt{P_c P_s}}{\Delta\nu} \delta f = D \delta f \quad (3.11)$$

where  $D \equiv -\frac{8\sqrt{P_c P_s}}{\Delta\nu}$  is called the "frequency discriminant" and effectively describes the slope of the PDH error signal in the region of interest - near the resonance of the reference cavity.

This linearity demonstrated in equation 3.11 is important, as it allows for the resulting PDH error signal to be fed into a servo loop filter (usually a PI or PID controller) to either adjust the laser cavity length via a intracavity piezoelectric transducer or, in the case of semiconductor lasers, the current fed into the laser diode.

The shot noise floor is a quantum noise effect caused by the discrete nature of light (i.e. photons) and places a fundamental lower bound on the optical intensity noise. The shot

noise power spectral density (PSD) of the signal incident on the reference cavity-reflected light photodiode is [30]:

$$S_e(f) = \sqrt{2 \frac{hc}{\lambda} [2P_s + P_{c,refl}]} \quad (3.12)$$

where  $h$  is Plank's constant,  $P_s$  is the power present in one sideband and  $P_{c,refl}$  is the carrier power reflected from the reference cavity that is incident on the photodetector. Note that the shot noise PSD is flat, as is always the case.

Thus, 3.12 places a lower bound on the frequency resolution of the setup by taking into consideration the unavoidable *shot noise limit*. The shot noise limit results from a quantum noise effect where the noise in the photons hitting the photodetector become large-enough compared to the actual signal (i.e. real information about the state of the system) such that the signal to noise ratio becomes too low to contain any useful data.

### 3.1.2 The Hänsch-Couillaud Technique

Another frequency stabilization technique which is related to the PDH method, albeit less popular for frequency stabilization, was first published in 1980 by Hänsch and Couillaud [31]. In the Hänsch-Couillaud technique (figure 3.4), linearly polarized light from a CW laser is reflected off of a confocal reference cavity which contains an intracavity linear polarizer, rotated at an angle  $\theta$ .

To avoid feedback into the CW laser resonator, the reference cavity is positioned off-axis, so that the reflected light off of the cavity can be directed towards a polarization analyzer. The incoming light from the CW laser can be decomposed by the following set of relations [31]:

$$\begin{aligned} E_{\parallel}^i &= E^i \cos \theta \\ E_{\perp}^i &= E^i \sin \theta \end{aligned} \quad (3.13)$$

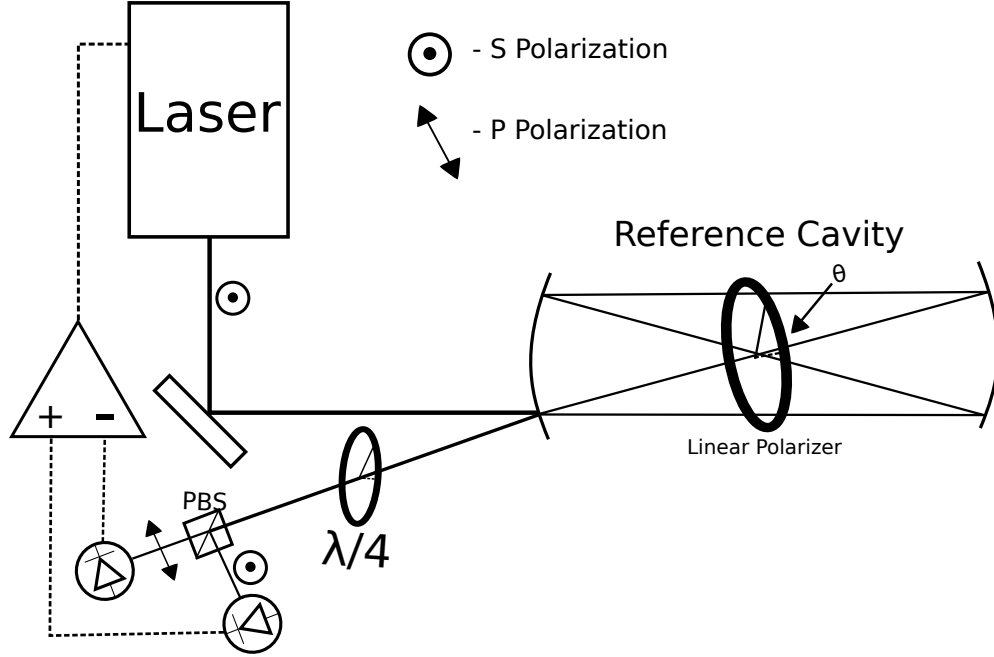


Figure 3.4: The Hänsch-Couillaud setup as described in the original 1980 paper. Note the similarities in experimental design to the PDH technique (figure 3.1).

where  $E_{\parallel}^i$  and  $E_{\perp}^i$  are the incident electric field vectors for the components parallel and perpendicular to the intracavity polarizer axis, respectively.

The parallel component of the incident electric field will "see" the reference cavity as low-loss and undergo a frequency-dependent phase shift during a roundtrip. The perpendicular component simply serves as a reference, as it cannot couple into the cavity at all and is *entirely* reflected by the first cavity mirror. Therefore, any difference in the change of phase undergone by the two components during reflection off of the cavity will translate into an elliptically polarized reflected beam. It is trivial to show that the complex parallel and perpendicular components of the reflected beam can be represented by the following [31]:



$$\begin{aligned}
E_{\parallel}^r &= E_{\parallel}^i \left[ \sqrt{r_1} - \frac{t_1}{\sqrt{r_1}} \frac{Re^{i\delta}}{1 - Re^{i\delta}} \right] \\
&= E_{\parallel}^i \left[ \sqrt{r_1} - \frac{t_1 R}{\sqrt{r_1}} \frac{\cos(\delta) - R + i \sin(\delta)}{(1 - R)^2 + 4R \sin^2(\frac{\delta}{2})} \right] \\
E_{\perp}^r &= E_{\perp}^i \sqrt{r_1}
\end{aligned} \tag{3.14}$$

where  $r_1$  and  $t_1 \equiv 1 - r_1$  are the reflectivity and transmissivity of the first cavity mirror, respectively,  $\delta$  is the phase difference between waves in consecutive round-trips and  $R < 1$  is the amplitude ratio between consecutive round trips - a parameter which accounts for the cavity losses due to the intracavity polarizer and the two additional reflections which are needed for an off-axis reference cavity. The  $R$  parameter is related to the finesse of the reference cavity by:  $\mathcal{F} = \frac{\pi\sqrt{R}}{(1-R)}$  - note that this is equivalent to equation 2.26 for the special case of two cavity mirrors with equal reflectivity values.

Equation 3.14 shows that if the incoming beam from the CW laser is exactly on-resonance with the cavity, i.e.  $\delta = 2\pi m$  - where  $m$  is an integer, then both reflected components are entirely real and thus maintain the same phase and a linear polarization (albeit rotated from the incident beam). However, when the incident beam is off-resonance, i.e.  $\delta \neq 2\pi m$ , the parallel component of the reflected electric field acquires an imaginary part which introduces a phase shift relative to the perpendicular component of the reflected electric field. This phase shift is what leads to the aforementioned elliptical polarization, the degree of which is determined by the distance from resonance and the direction of which, i.e. "handedness", is determined by the side of resonance the incoming beam is on. Therefore, all of the information needed to create an error signal to feed back to the laser is present in the reflected beams. Thus, the reflected beam is directed into the polarization analyzer (figure 3.4), which consists of a quarter-wave plate rotated by  $45^\circ$  relative to the fast axis of the beam, a  $45^\circ$  linear polarizer, a polarizing beamsplitter, two photodetectors and a differential amplifier. When the reflected beam passes through the rotated quarter-wave plate, the polarization of the reflected beam is transformed into two, linearly polarized, orthogonal waves. Then, passing

through the linear polarizer oriented at  $45^\circ$  forces the projection of the parallel component linearly polarized light to be parallel to the table, and likewise, forces the projection of the perpendicular component of the linearly polarized light to be perpendicular to the table - this step is purely for ease of alignment of the subsequent polarizing beamsplitter (which can easily be aligned relative to the table). When the beam passes through the polarizing beamsplitter, the linearly polarized parallel and perpendicular components are directed into their respective photodetectors. The signals from these photodetectors are then sent into a differential amplifier which, after the photodetectors have been properly balanced, lead to a error signal (figure 3.5) which looks similar to the PDH error signal (figure 3.3), but without the contribution from any phase modulation sidebands.

This error signal is the difference between the signals from the two balanced photodetectors and is represented mathematically by the following [31]:

$$I_a - I_b = I^{(i)} 2 \cos(\theta) \sin\left(\theta \frac{t_1 R \sin(\delta)}{(1 - R)^2 4 R \sin^2(\frac{1}{2}\delta)}\right) \quad (3.15)$$

where  $I^{(i)}$  is the intensity of the beam at the entrance to the polarizing beamsplitter and  $I_a$  and  $I_b$  are the intensities of the light incident on the two balanced photodetectors.

As is apparent in equation 3.15, the error signal crosses the DC point when the CW laser is exactly on resonance (i.e.  $\delta = 2\pi m$ ). Furthermore, the presence of the  $\sin(\delta)$  term in the Hänsch-Couillaud error signal demonstrates that it is asymmetric around resonance. Just as with the PDH stabilization technique, the Hänsch-Couillaud error signal can be used with a servo loop filter to feedback to either the laser current or laser cavity length in order to lock the frequency of the CW laser's output.

Although both the Hänsch-Couillaud and the Pound, Drever, Hall techniques for laser frequency stabilization have the same objective, the Hänsch-Couillaud has the advantage of not requiring the use of an electro-optic modulator which generates sidebands that could be undesirable for some applications. However, the Hänsch-Couillaud technique suffers

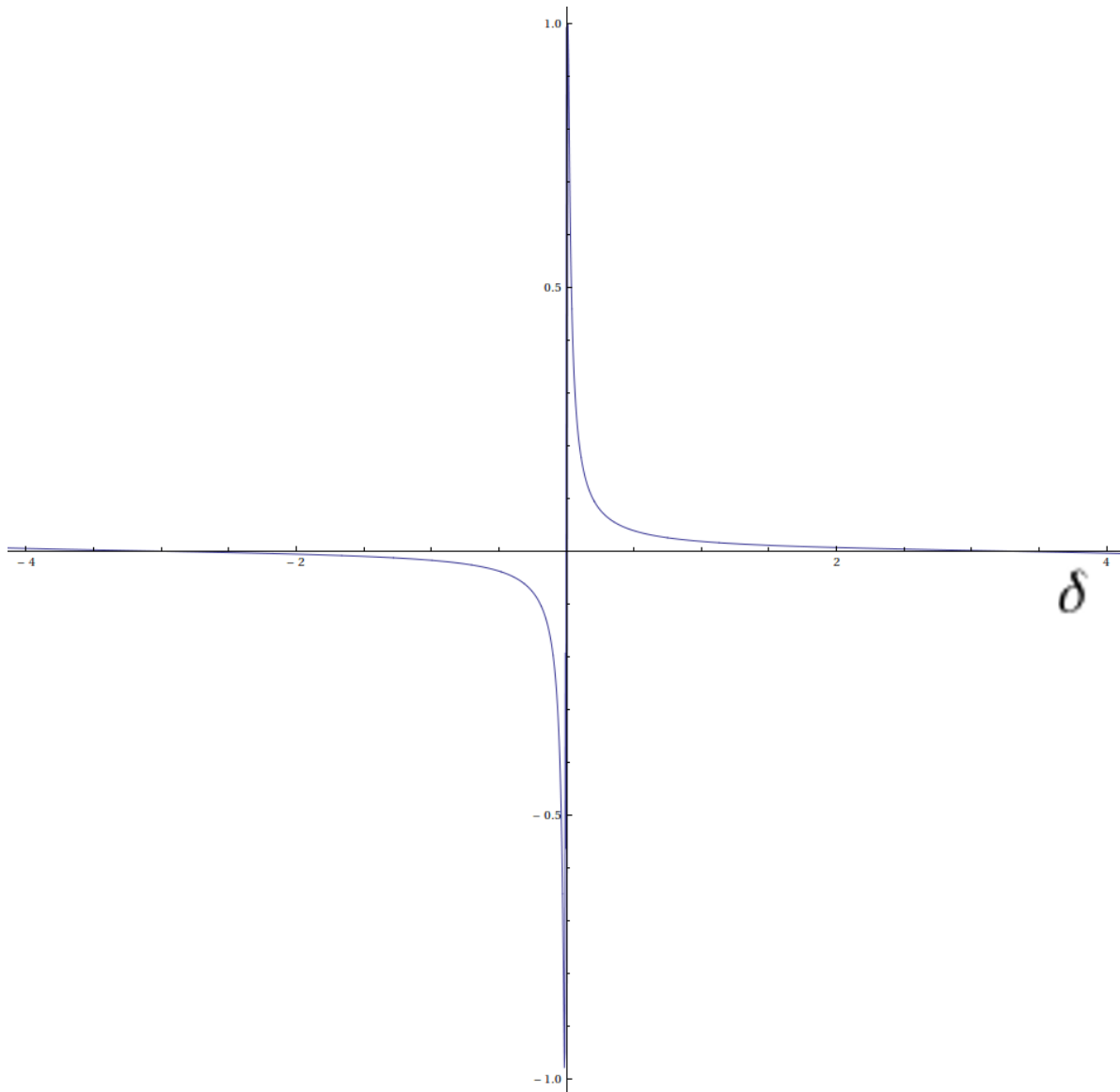


Figure 3.5: The normalized Hänsch-Couillaud error signal as a function of the deviation from resonance,  $\delta$ . Note that the important property of asymmetry around resonance is present, just as can be seen in the PDH error signal (figure 3.3).

from several drawbacks which the PDH technique developers sought to rectify. First, the Hänsch-Couillaud technique requires the use of an intracavity polarizer which introduces extra losses in the reference cavity, as described by equation 3.14. Second, the Hänsch-Couillaud technique requires that the two photodetectors used to pick up the beams after the polarizing beamsplitter must be perfectly balanced - a rather tedious task. Third, the alignment of

the polarizing components in the Hänsch-Couillaud technique is very sensitive, for example, the angle of the intracavity polarizer must be carefully balanced between  $\theta = 45^\circ$  (where the error signal in equation 3.15 is maximized) and  $\theta = 0^\circ$ , where the error signal vanishes according to equation 3.15, but the signal-to-noise (SNR) is maximized (assuming that the intensity noise of the CW laser is the dominant noise source) [31]. These problems with the Hänsch-Couillaud method are a large part of the reason that the Pound, Drever, Hall method has become the preferred technique for CW laser frequency stabilization over the last several decades.

### 3.1.3 Stabilization Techniques for Modelocked lasers

Although the Pound, Drever, Hall technique presented in section 3.1.1.1 has become the preferred technique for the frequency stabilization of CW lasers, effective techniques for their modelocked counterparts have been developed in recent years [32, 5]. Two such modelocked laser stabilization techniques are presented in this section.

#### 3.1.3.1 Full Frequency Comb Lock

As discussed in section 1.1, modelocked lasers (see section 2.2.1) produce pulses, which in the frequency domain have many equally-spaced components which form the teeth of a device known as a frequency comb. As equation 1.1 illustrates, both the repetition rate,  $f_r$ , and the carrier envelope offset frequency,  $f_0$ , must be stabilized to a stable reference in order to produce a fully stabilized frequency comb. One such full frequency comb lock is described in a 2000 paper by Jones et al. [32], where a self-referencing method (figure 3.6) is used to lock the carrier envelope offset frequency, which avoids the necessity of an additional stable reference oscillator, such as a CW laser, which would need to be stabilized itself and operates at optical frequencies which are generally  $> 10^6$  times larger than the repetition rate [32].

Essentially, the self referencing method described in Jones et al. first uses an optical fiber to induce self-phase modulation (SPM) and other nonlinear effects which broaden the

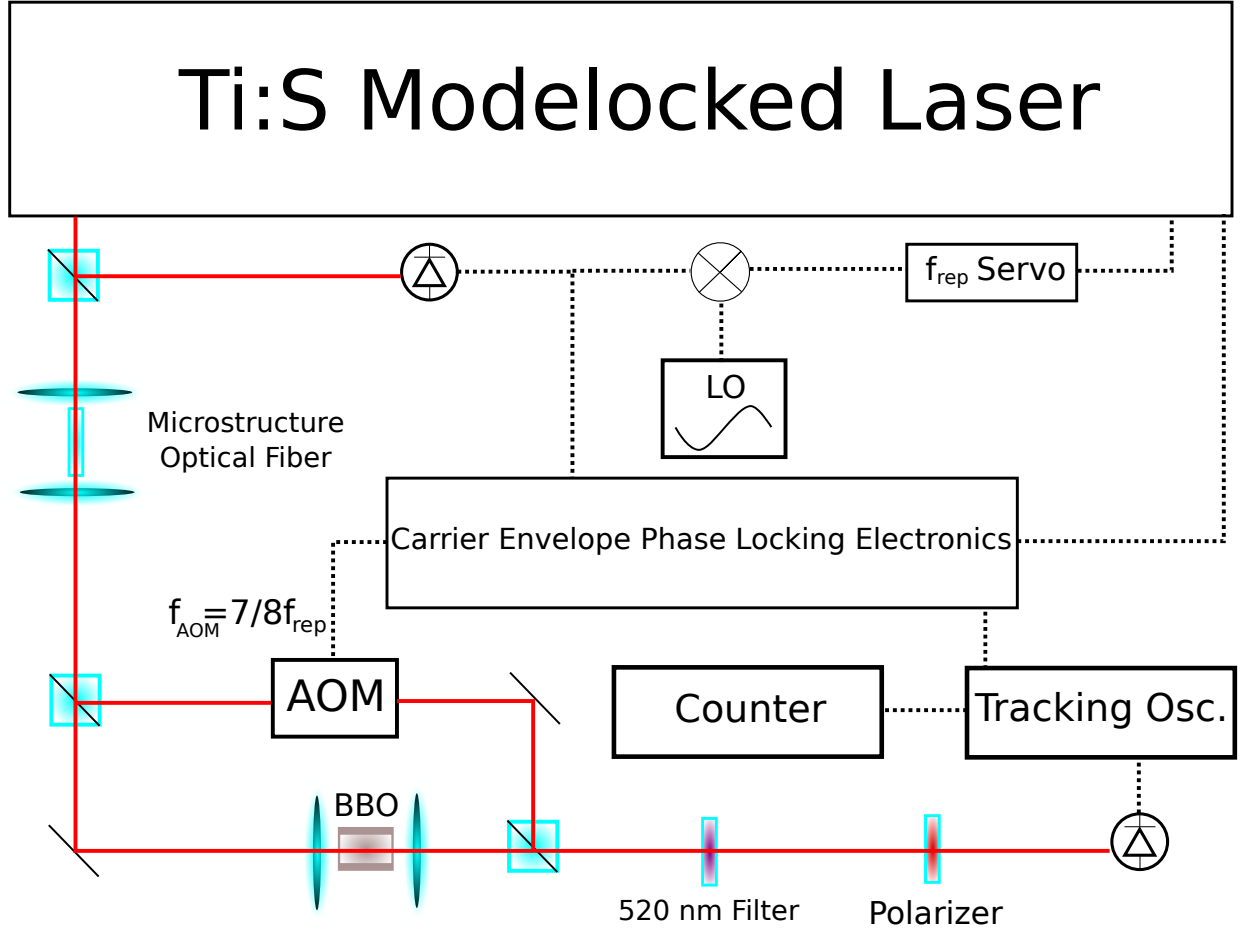


Figure 3.6: The self-referencing (f-2f) scheme setup as described by Jones et al.

spectrum of the pulses so that an optical octave is achieved, i.e. where at least the lowest frequency present in the pulse's spectrum has a corresponding frequency component that is double this lowest frequency. For example, the output pulses of the Ti:Sapphire laser used in Jones et al. have a center frequency of  $\approx 350$  THz and a spectral bandwidth of  $70 \text{ nm} \equiv 30 \text{ THz}$  [32]. Manifestly, this is far less than a full optical octave and so an optical fiber is required to broaden the spectrum width to  $\approx 615 \text{ nm} \equiv 488 \text{ THz}$ , which contains several optical octaves. Then, one of the lower optical frequencies is selected, which can be represented by the following:

$$f_n = n f_r + f_0 \quad (3.16)$$

where  $f_n$  is the  $n$ th comb tooth frequency and is on the low ("red") end of the comb's optical spectrum.

Then, the comb tooth frequency,  $f_n$ , is frequency doubled via second-harmonic generation (SHG) by a nonlinear crystal and can then be described by:

$$2f_n = 2nf_r + 2f_0 \quad (3.17)$$

This signal can then be fed into a heterodyne along with the corresponding "blue"  $f_{2n}$  tooth signal directly from the optical frequency comb. The result of this mixing process, after proper filtering, is:

$$2f_n - f_{2n} = (2nf_r + 2f_0) - (2nf_r + f_0) = f_0 \quad (3.18)$$

Thus, the carrier envelope offset frequency,  $f_0$ , can be measured and subsequently stabilized via feedback to the modelocked laser - typically to zero, i.e.  $f_0 = 0$ . Note that the experimental setup (figure 3.6) for this self-referencing scheme is relatively complex and is described in the above non-detailed manner for the sake of brevity.

Finally, after the carrier envelope offset frequency is stabilized, the repetition rate of the modelocked laser can be stabilized by comparing a high harmonic of a highly-stable RF frequency reference (or alternatively, a PDH-stabilized CW laser reference, as in Quinlan et al. [7]) to the repetition rate,  $f_r$ , and utilizing a feedback loop with an intracavity piezoelectric transducer mounted on a mirror to adjust the cavity length and stabilize the repetition rate [32]. Thus, as both the carrier offset envelope frequency,  $f_0$ , and the repetition rate,  $f_r$ , are known and stabilized, the frequency comb becomes a powerful tool for absolute frequency metrology, owing to the fact that (in accordance with equation 1.1) the optical frequency of each comb tooth is now precisely known.

Although the above technique fully stabilizes a frequency comb, which enables many applications that require an absolute frequency reference, the drawbacks are that it is a

relatively complex setup which requires many components and is difficult to operate for extended periods of time.

### 3.1.3.2 Differential Frequency Comb Lock

A second technique for the stabilization of modelocked lasers by Swann et al. [5] seeks to reduce the complexity of the full frequency comb lock presented in the previous section. In the modelocked laser stabilization technique described in the 2011 paper by Swann et al. (shown in figure 3.7), a femtosecond Erbium fiber laser (center wavelength,  $\lambda_{c,MLL} \approx 1555$  nm) is stabilized by first simultaneously locking two CW lasers to a stable reference cavity via the PDH technique.

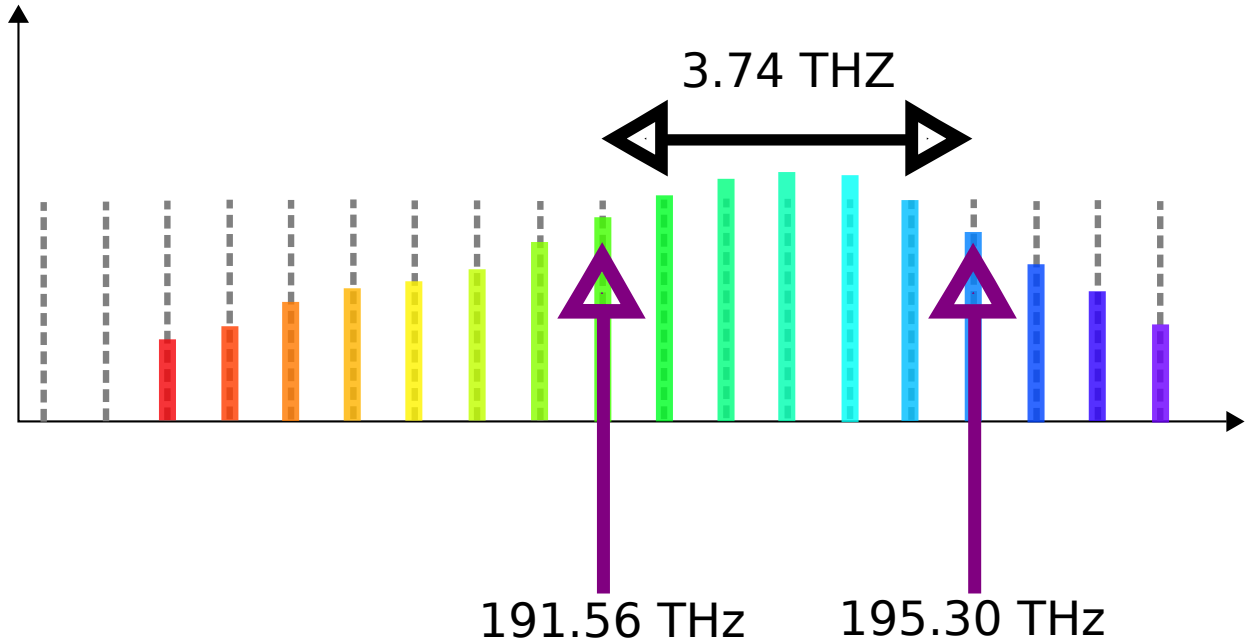


Figure 3.7: The differential frequency comb lock setup described in Swann et al. The above shows the differential comb lock in the frequency domain.

The output of the Erbium femtosecond fiber laser has a bandwidth of  $\approx 30$  nm = 3.74 THz, thus one of the CW lasers is stabilized at  $\lambda_{c,CW1} = 1535$  nm = 195.30 THz and the other is stabilized at  $\lambda_{c,CW2} = 1565$  nm = 191.56 THz [5]. Then, the two PDH-stabilized CW lasers are phase locked to the corresponding two teeth of the frequency comb. This

automatically locks both the spacing of the teeth in the frequency comb, i.e. the repetition rate, and the carrier envelope offset. Thus, the comb is fully stabilized without the complexity associated with using a nonlinear fiber for supercontinuum generation and a  $f$  to  $2f$  self-referencing scheme. However, the main drawback of this technique compared to the full frequency comb stabilization method presented in section 3.1.3.1 is that the stabilization "moment arm" is 3.74 THz as opposed to the "moment arm" of the full comb lock, which would be  $\approx 200$  THz for an Erbium fiber femtosecond laser [5]. This decreases the sensitivity of the optical locks to the excess phase noise, compared to the full comb lock, by a factor of  $\left(\frac{3.74 \text{ THz}}{200 \text{ THz}}\right)^2 \approx \frac{1}{2500}$  [5]. This effectively lowers the quality factor (defined as:  $Q \equiv \frac{f_r}{\Delta f}$ ) of the resonance used for the comb lock. This lower quality factor places a fundamental limitation on the bandwidth of the lock that can be implemented in this setup. In addition, modelocked fiber lasers are generally much noisier than their modelocked bulk counterparts, thus a coherent lock requires the use of an intracavity electro-optic modulator (EOM). Therefore, the differential frequency comb lock can only be realized with the use of fiber modelocked lasers, as an intracavity fiber-coupled waveguide modulator can be used as the EOM, allowing for feedback bandwidths on the order of a MHz [5]. However, due to the superior robustness of fiber-based lasers, the differential comb lock is, in general, better suited for field-deployable or portable modelocked laser systems.

### 3.2 Experimental Setup

The PDH-based experimental setup presented in this thesis is an attempt to achieve low phase noise, and therefore timing jitter, performance through an experimental setup which is even less complex and requires fewer components than either the full frequency comb lock presented in section 3.1.3.1 or the differential frequency comb lock presented in section 3.1.3.2. This setup is achieved by using a fiber-based Pound, Drever, Hall stabilization technique which has been adapted for use with a modelocked, free space, bulk erbium-doped ytterbium (Er:Yb) modelocked laser with a repetition rate of 500 MHz. The details of the experimental



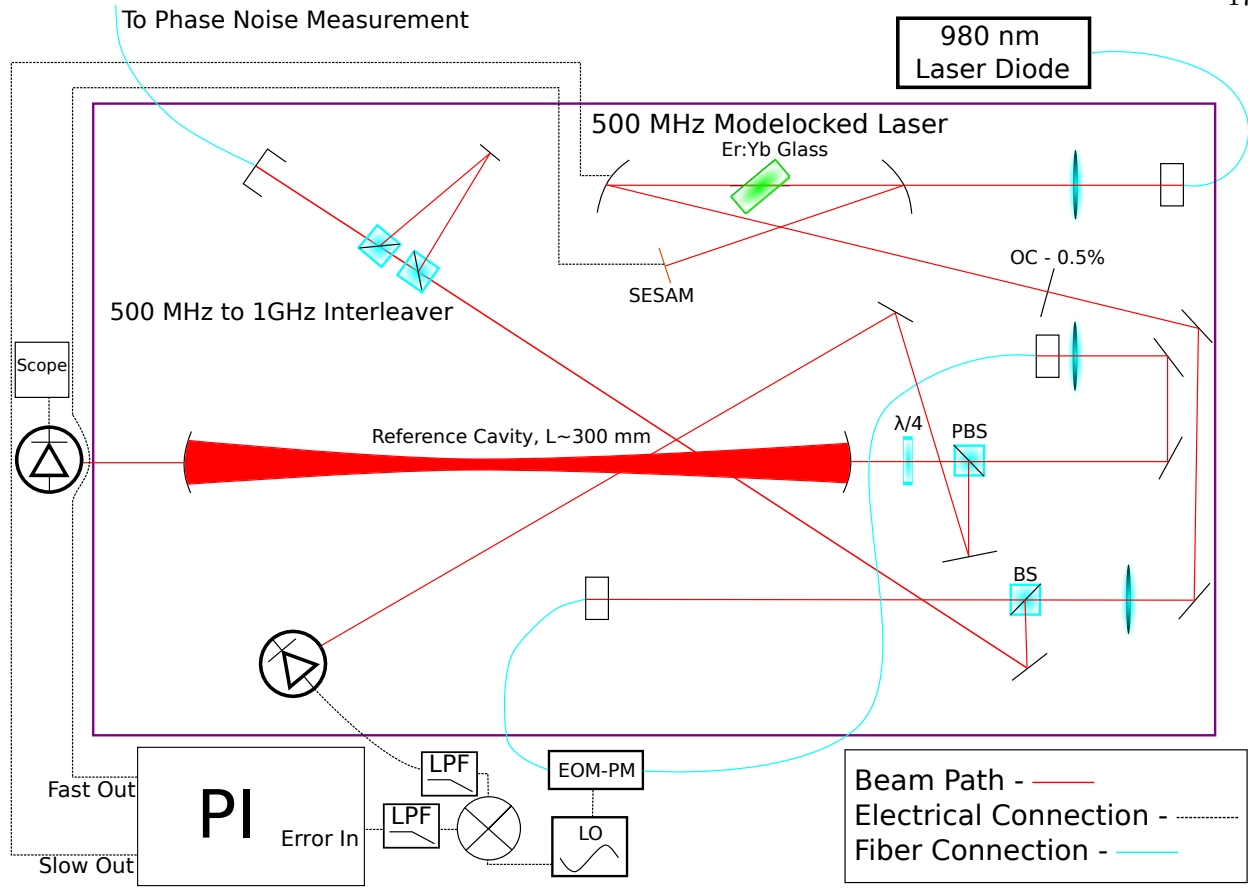


Figure 3.8: A diagram of the experimental setup. The purple rectangle represents the acrylic box's boundaries. The photodetector and (oscillo)scope on the left-hand side of the diagram is only used for monitoring the transmission through the cavity and is helpful, though not essential, for the cavity lock.

setup are described in the following sections. The experimental setup is shown in figure 3.8.

### 3.2.1 500 MHz Modelocked Laser

A continuous-wave ( $\lambda_c \approx 1560$  nm), bulk (i.e. doped glass gain medium), free-space (i.e. operates in open-air) laser was first constructed using an erbium-doped ytterbium gain medium (Kigre, Inc. - QX/Er - Datasheet: Appendix A) and was pumped by a 980 nm laser diode (Gooch and Housego - Model #: D1306077). The laser resonator has a folded "X" design and an asymmetric long and short arm, as shown in figure 3.8. A 0.5% output coupler (OC) was used at the end of the long arm to couple light from the laser resonator

to the output. After tuning the CW laser to reduce intracavity dispersion losses, the end mirror in the short arm was replaced by a semiconductor saturable absorber mirror (SESAM). The folded "X" design was necessary to simultaneously achieve the correct mode size at the center of the gain medium and provide a tight focus at the SESAM - necessary to achieve the saturation behavior described below. The exact dimensions of the cavity were determined through the use of ABCD matrices for Gaussian beams [33], a screen shot showing the final laser dimensions from this ABCD calculation in *Mathematica* is shown in figure 3.9.

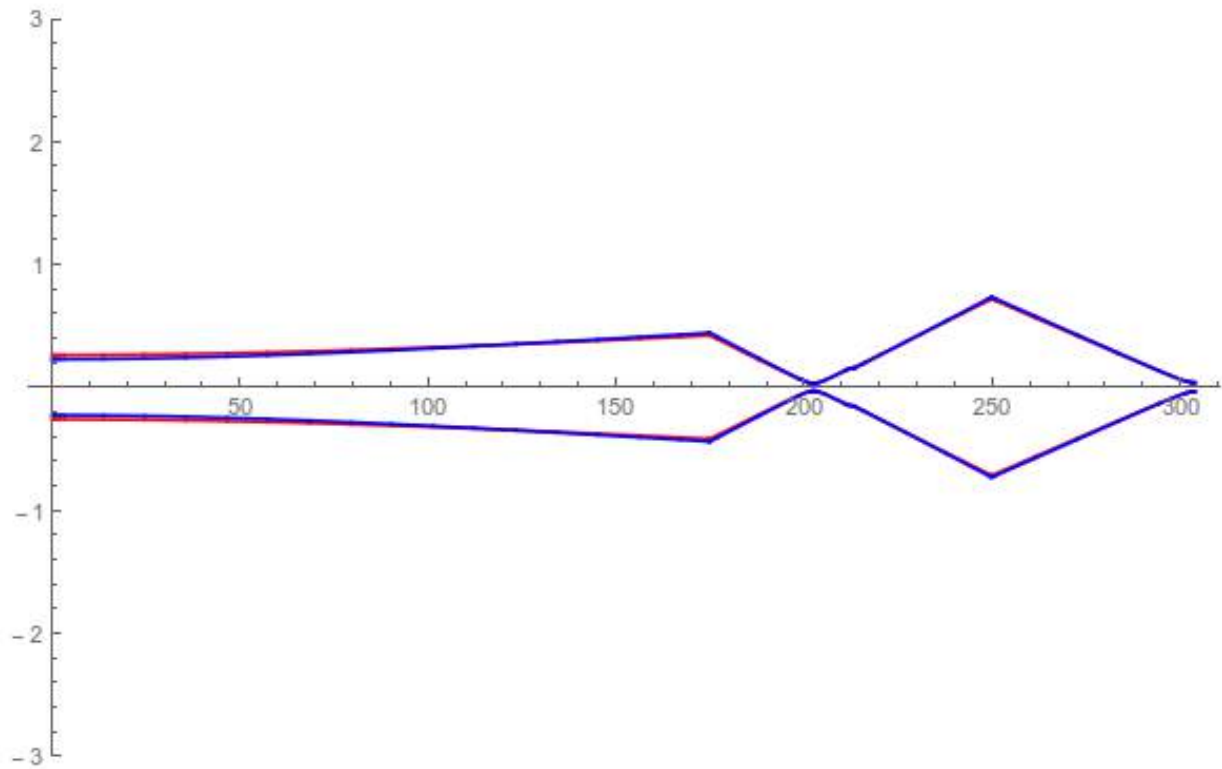


Figure 3.9: An ABCD calculation screen shot for 500 MHz modelocked laser. The red and blue lines represent the transverse and longitudinal modes of the laser. The final dimensions of the laser cavity were 73 mm for the distance between the two curved mirrors, 54 mm for the short arm (with the SESAM) and 175 mm for the long arm (with the output coupler). Note that the transverse and longitudinal modes must be overlapped for lasing to occur. The *Mathematica* document used to generate this plot was implemented by Dr. Chien-Chung Lee.

The SESAM used here is a combination of the properties of a slow and fast saturable

absorber and was used to passively modelock the laser to achieve pulsed operation, as described in section 2.2.1. The SESAM is constructed from a single InGaAs quantum well, which is followed by a Bragg stack composed of alternating quarter wave plates made from GaAs and AlAs. This design allows for inter-band transitions at the InGaAs well (i.e. recombination from the conduction band to the valence band), which leads to the slow behavior of the SESAM and allows for self-starting modelocking behavior [34]. When the InGaAs well is partially saturated, the conduction band contains electrons which lead to the effects of electron-electron and electron-phonon scattering, as well as transitions from the conduction band to the defect states present between the valence and conduction bands of the single quantum well (these defect states are purposeful and are achieved by growing the InGaAs at low temperature). These effects occur on a much shorter time scale than the inter-band transitions, and therefore, provide the fast saturable absorber properties that partially allow for the formation of femtosecond pulses [34]. Lastly, the Bragg stack behind the InGaAs quantum well ensures that the SESAM essentially becomes a nearly 100% reflecting mirror when the intracavity pulse energy is high enough to saturate the quantum well. Furthermore, the erbium-doped ytterbium glass used as the gain medium in this laser's construction introduces anomalous (i.e. negative) dispersion in the resonator, which is generally necessary for the generation of ultrashort pulses according to the theory of soliton modelocking [22], but will not be discussed in detail here for the sake of brevity. After adjusting the position and angle of the SESAM to achieve maximum output power, the output of the modelocked laser was loosely coupled into a fiber and measured by an optical spectrum analyzer (OSA). The OSA measurement, as well as a RF analyzer measurement, showed the following parameters of the modelocked laser:

$$\begin{aligned}
\lambda_c &= 1551.66 \text{ nm} \\
\Delta\lambda &= 12.98 \text{ nm} \\
f_r &= 496.8 \text{ MHz} \\
P_{out} &\approx 57 \text{ mW}
\end{aligned}
\tag{3.19}$$

where  $\Delta\lambda$  is the spectral bandwidth of the pulses emitted from the modelocked laser.

The measured repetition rate of 496.8 MHz indicates that the final length of the laser resonator, through application of equation 2.10, was  $L \approx 302 \text{ mm}$ . The output coupler mirror was mounted on a precision stage so that the repetition rate could be tuned easily. Finally, the transverse mode appeared to be entirely a  $\text{TEM}_{0,0}$  mode, as desired, by visual inspection.

### 3.2.2 Electro-optic Modulator

The setup uses a fiber-based electro-optic phase modulator. Initially, a bulk electro-optic phase modulator was constructed for use in the setup, but problems with phase modulation (PM) to amplitude modulation (AM) were noticed, thus a fiber-based PDH scheme was pursued instead. Although losses from coupling are inevitably introduced when using a fiber-based electro-optic phase modulator, the advantage of fiber-based electro-optic phase modulators over their free-space counterparts are a higher bandwidth and far less PM to AM conversion. The fiber-based electro-optic phase modulator used in this setup was a lithium niobate ( $\text{LiNbO}_3$ ) crystal modulator from EO-Space (Model #: PM-0K5-10-PFA-PFA, Datasheet: Appendix B). The electro-optic phase modulator was driven with a  $\Omega = 8 \text{ MHz}$  peak-to-peak amplitude of 8 V, which transferred  $\approx 15.57\%$  of the optical power to *each* sideband according to measurements using the transmitted power through the reference cavity on resonance (a reasonable measurement technique, given that the sidebands were well-outside of the reference cavity bandwidth, see equation 3.21).

### 3.2.3 Stable Reference Cavity

The reference cavity constructed for this setup is composed of two concave mirrors (reflectivity  $\approx 99.3\%$  at  $\lambda = 1551.66$  nm, LayerTech - Coating Batch #: R1009002 and F115H010, (R1009002) Dielectric Coating Datasheets: Appendix C) in free-space near (see figure 3.8 for location in setup) the 500 MHz modelocked laser. The first - i.e. entrance - mirror of the cavity has a radius of curvature of 1000 mm and the second mirror of the cavity has a radius of curvature of 500 mm. Concave mirrors were chosen for this reference cavity in order to reduce undesirable mode degeneracy (described in section 2.4.2). Both mirrors have a substrate made from fused silica.

The reference cavity with designed with a length of  $L_{ref} \approx 302$  mm so as to match the free spectral range of the modelocked Er:Yb laser. The second mirror of the reference cavity was mounted on a precision stage to allow easy tuning of the reference cavity length, and therefore, the resonances. With the above parameters, the finesse of the reference cavity can be estimated with equation 2.26:

$$\mathcal{F} = \frac{\pi(r_1 r_2)^{\frac{1}{4}}}{1 - (r_1 r_2)^{\frac{1}{2}}} = \frac{\pi\sqrt{.993}}{1 - .993} \approx 447.23 \quad (3.20)$$

Therefore, the linewidth of the reference cavity,  $\Delta\nu_{cav}$  can be estimated as:

$$\Delta\nu_{cav} = \frac{\text{FSR}}{\mathcal{F}} = \frac{496.8 \text{ MHz}}{447.23} \approx 1.11 \text{ MHz} \quad (3.21)$$

The incoming beam was mode-matched to the reference cavity (through the use of ABCD calculations [33]), to maximize the coupling efficiency, using a lens placed near the output of the fiber link (see figure 3.8). To measure the coupling efficiency, the DC value (with the reference cavity blocked) of the reference cavity-reflected power photodetector signal was compared to the photodetector signal with the cavity on-resonance, by scanning the

modelocked laser cavity with the slow piezo. The results for this contrast were as follows:

$$\frac{\text{Transmission Peak Voltage}}{\text{DC Voltage}} = \frac{76 \text{ mV}}{254 \text{ mV}} = .2992 \approx 30\% \quad (3.22)$$

Thus, the coupling efficiency of light into the cavity was measured to be  $\approx 30\%$ .

Dividing equation 3.12, the shot noise of the reflected power falling on the photodiode, by the frequency discriminant,  $D$  (equation 3.11), yields the apparent frequency shot noise for the PDH setup [30]:

$$\begin{aligned} S_\nu(f) &= \left[ \frac{\sqrt{hc^3}}{8} \frac{1}{\mathcal{F}L\sqrt{\lambda\eta P_{tot,PD}}} \right]^2 \\ &= \left[ \frac{\sqrt{hc^3}}{8} \frac{1}{(447.23)(302 \times 10^{-3} \text{ m})\sqrt{(1551.66 \times 10^{-9} \text{ m})[(.25)3.9 \times 10^{-3} \text{ W}]}} \right]^2 \quad (3.23) \\ &= 1.011 \times 10^{-5} \frac{\text{Hz}^2}{\text{Hz}} \end{aligned}$$

where  $L$  is the length of the reference cavity,  $\mathcal{F}$  is the finesse of the reference cavity,  $P_{tot,PD}$  is the total power reflected from the reference cavity as measured by the photodiode and  $\eta$  is an empirically-determined correction factor which accounts for the imperfect transverse mode mismatch and the difference between the reflected carrier and sideband power. This calculation places a *lower* bound on the shot noise limit, due to the fact that there are other contrast factors which can potentially limit the effective carrier power, such as the amplitude of the beat note between the reflected carrier and sidebands. However, these factors are generally small compared to the parameters considered above, thus, equation 3.23 provides a reasonable lower bound for the shot noise limit in this PDH setup.

Furthermore, this shot noise limits the lock's sensitivity to the reference cavity length when locked to the modelocked laser, thus the length noise density, under shot noise limited conditions, would be [30]:

$$S_L(f) = \frac{L}{\nu} S_\nu(f) = \frac{(302 \times 10^{-3} \text{ m})}{(193.21 \text{ THz})} (1.011 \times 10^{-5} \frac{\text{Hz}^2}{\text{Hz}}) = 1.58 \times 10^{-20} \frac{\text{m}}{\text{Hz}} \quad (3.24)$$

which represents the smallest distance the laser cavity length could change by and be recognized by the feedback loop under shot noise-limited conditions - in layman's terms: with every part of the setup operating ideally.

### 3.2.4 Environmental Isolation

To minimize the effects of acoustic vibrations, a series of environmental isolation techniques were used in this setup, which are described in this section. As with all of the experiments in the Schibli Lab, the setup was constructed on top of a high-performance Laminar flow isolation table (Newport: S-2000 series) which is suspended by a cushion of air. Furthermore, this setup was built on an optical breadboard (Newport, Model #: PG-12-2 1712963) which contains viscous damping materials and was in turn placed on top of an acoustic-damping piece of flat foam which introduces an impedance mismatch for acoustic waves between the massive, dense breadboard and the solid material under it. Lastly, the breadboard and foam was placed inside of a 1 inch-thick acrylic box with a removable lid. A photograph of this environmental isolation setup is provided for clarity in figure 3.10.

### 3.2.5 Electronics

For this setup, a low-noise, passive photodetector was constructed to pick up the reflected signal from the passive reference cavity. Furthermore, a commercial, fixed-gain photodetector (Thorlabs - Model #: PDA10CF) is used to monitor the transmission through the reference cavity and was placed outside of the acrylic box to avoid a thermal contribution from the powered electronics within the photodetector. The local oscillator signals are provided by a waveform generator (Rigol - Model #: DG1022) operating its two outputs in phase-aligned mode. The waveform generator also allows for tuning of the phase of one

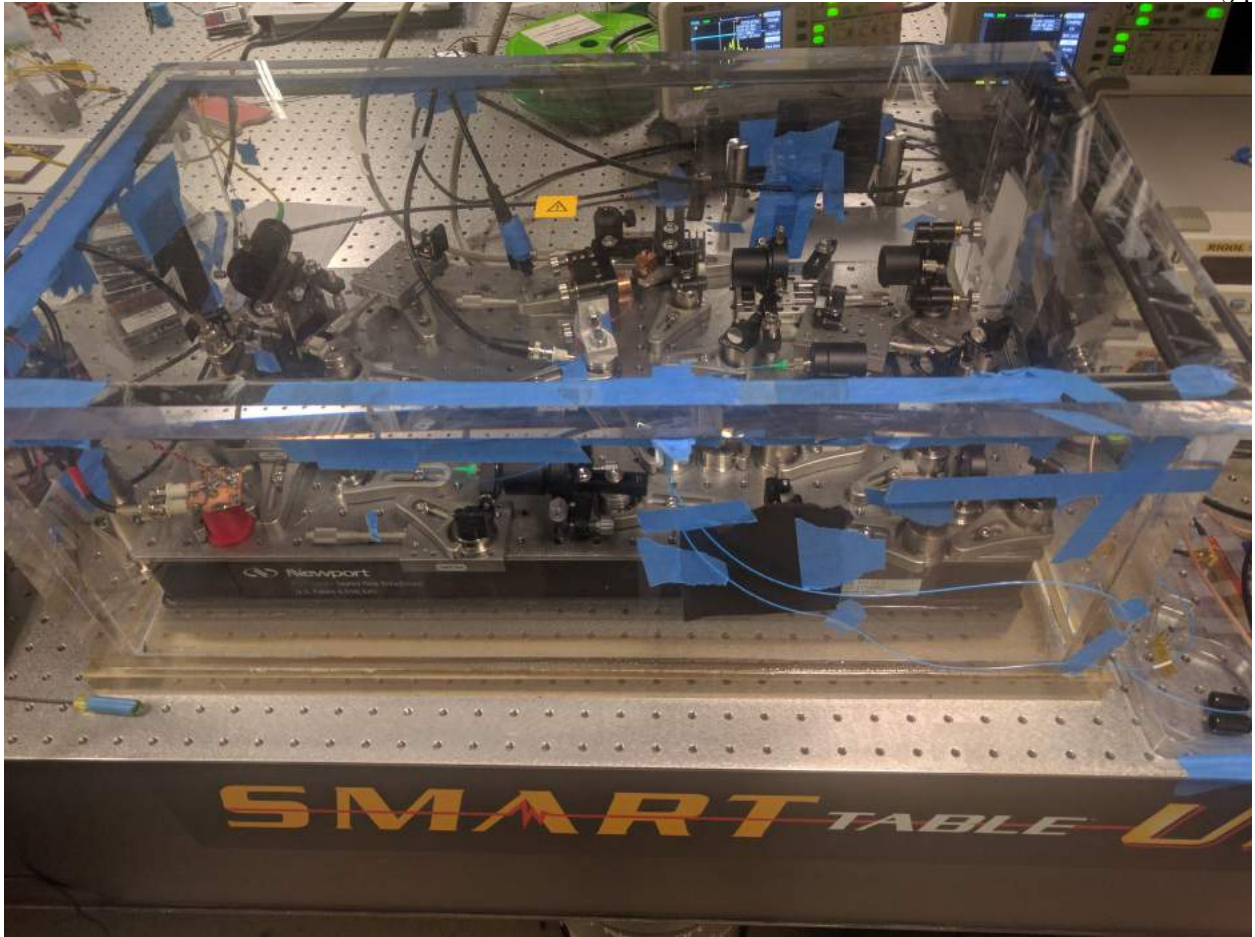


Figure 3.10: The experimental environmental isolation setup described in section 3.2.4.

or both synchronized outputs, thus making it easy to empirically compensate the delays in the electrical signals by simply looking at the error signal while adjusting the relative phase between the local oscillator line to the mixer and electro-optic phase modulator. The final error signal was obtained by filtering the output of the mixer (Minicircuits: Model #: SRA-6+) using a low-pass filter (Minicircuits: Model #: BLP 5+) with a 3dB corner of 5 MHz to remove the residual carrier, as shown in equation 3.5. Furthermore, a low-pass filter (Minicircuits: Model #: BLP 15+) with a 3dB corner of 15 MHz was used at the output of the cavity-reflected power photodetector to reduce the high frequency noise.



### 3.2.5.1 Servo Loop Filter

A proportional-integrator (PI) servo loop filter was constructed from scratch specifically for this setup's PDH-based lock. The PI controller has both a fast and a slow output, allowing for a fast piezo mounted under the SESAM to make corrections for fast components in the error signal (i.e.  $\ll 1$  s) and a slow piezo mounted in the stage of the second curved mirror of the laser to make corrections for the slow components ( $> 1$  s) in the error signal, such as thermal drifts. The circuit diagram for the PI servo loop filter is provided in figure 3.11.

### 3.2.6 500 MHz to 1 GHz Interleaver

An interleaver was constructed (shown in figure 3.8) in order to double the carrier from  $\approx 500$  MHz to  $\approx 1$  GHz before coupling into a fiber to perform the phase noise measurement described in section 4.2.1. The interleaver consisted of two beamsplitter cubes and a delay line mirror mounted on a precision stage. The interleaver works by essentially using the delay line to insert an effective delay of half the pulse period, i.e.  $\tau_{\text{delay, effective}} = \frac{1}{2f_r}$ . This leads to an "interleaving" of the original pulse train and the delay line pulse train to create the desired 1 GHz carrier signal. The delay line was tuned by viewing the output of the interleaver on a RF spectrum analyzer using a fast photodetector and maximizing the 1 GHz carrier.

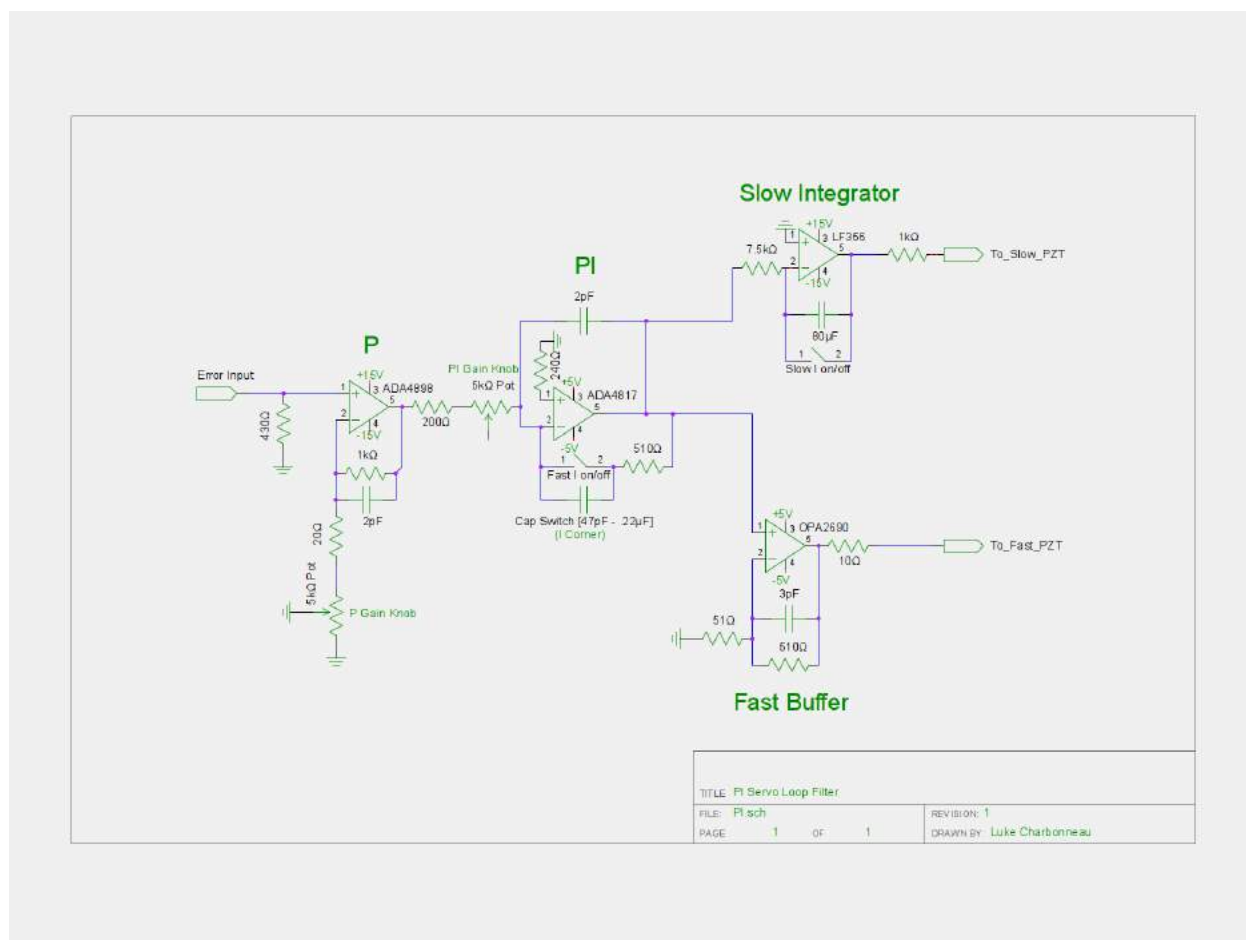


Figure 3.11: The circuit diagram for the PI servo loop filter.

## Chapter 4

### Results

#### 4.1 Lock Performance

The 500 MHz modelocked laser was locked to the passive reference cavity by first monitoring the transmitted power through the cavity and then scanning the laser cavity with the slow piezo mounted within the translation stage of the second curved mirror of the cavity. This allowed for the viewing of the reference cavity's resonances on an oscilloscope. The resonances visualized on an oscilloscope while scanning the laser cavity with the electro-optic phase modulator turned off and on are shown in figures 4.1 and 4.2, respectively.

At this point, the error signal could also be seen by viewing the output of the mixer (see figure 3.8) on another oscilloscope. The resulting error signal near resonance is shown in figure 4.3.

Then, the laser cavity scanning was stopped and the slow piezo in the laser cavity was manually adjusted until the strongest resonance was shown on the oscilloscope. Lastly, the fast, and subsequently, the slow integrator were switched on to engage the passive reference cavity lock. The fast piezo mounted under the SESAM damped all fast oscillations and ultimately determined the bandwidth of the lock, measured to be 188.7 kHz. The slow piezo mounted on a curved mirror in the laser cavity adjusted the cavity length to compensate for long-term drifts in the repetition rate of the modelocked laser, e.g. drifts caused by thermal changes in the room. The combination of the two separate feedback mechanisms allowed for the simultaneous damping of fast oscillations and long-term stability. In a test

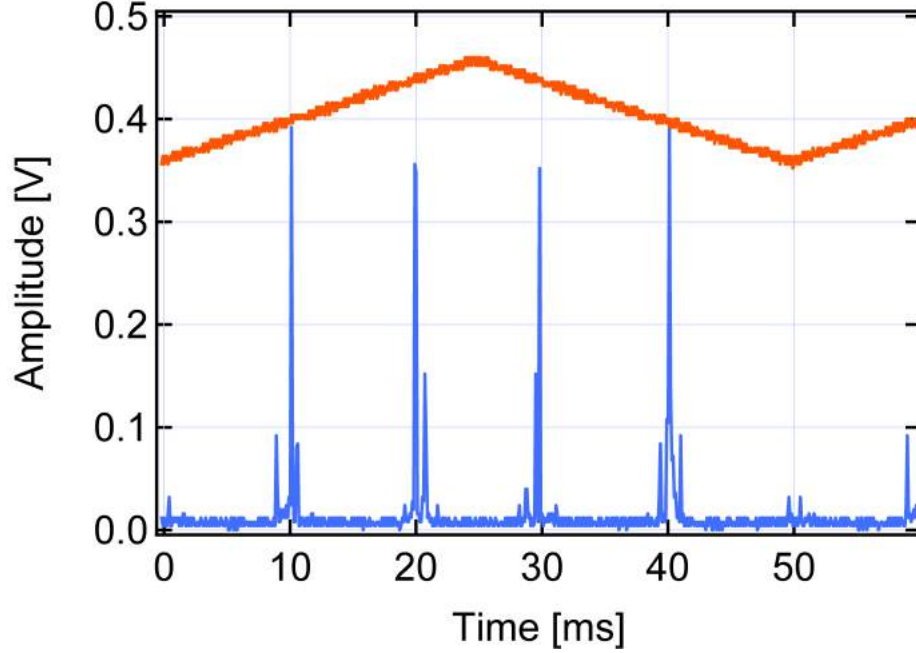


Figure 4.1: Passive cavity resonances with the electro-optic phase modulator turned off, i.e. no carrier sidebands. The red trace represents the scan driving voltage of the slow piezo, and is 10 Hz and 2 V<sub>pp</sub> (red curve not to scale). The smaller peaks seen in this figure are resonances of higher-order modes present in the reference cavity, but are much smaller than the fundamental resonances.

of the long-term stability of the reference cavity lock, the slow piezo was determined to drift by 0.153 V per hour, thus, given that the slow integrator has a maximum, single-sided voltage swing of 15 V, a lower bound on the long-term stability of the lock was estimated to be  $\approx 98$  hours. This is a very conservative lower bound, as the temperature changes in a room are bounded, and even more so if the breadboard is temperature stabilized. The transmission signal through the reference cavity while the lock was engaged, as visualized on an oscilloscope, is shown in figure 4.4.

## 4.2 Phase Noise Measurement

The ultimate goal of this setup was to minimize the timing jitter of a free-space modelocked laser in the least complex, and therefore most stable, manner possible. Thus, a

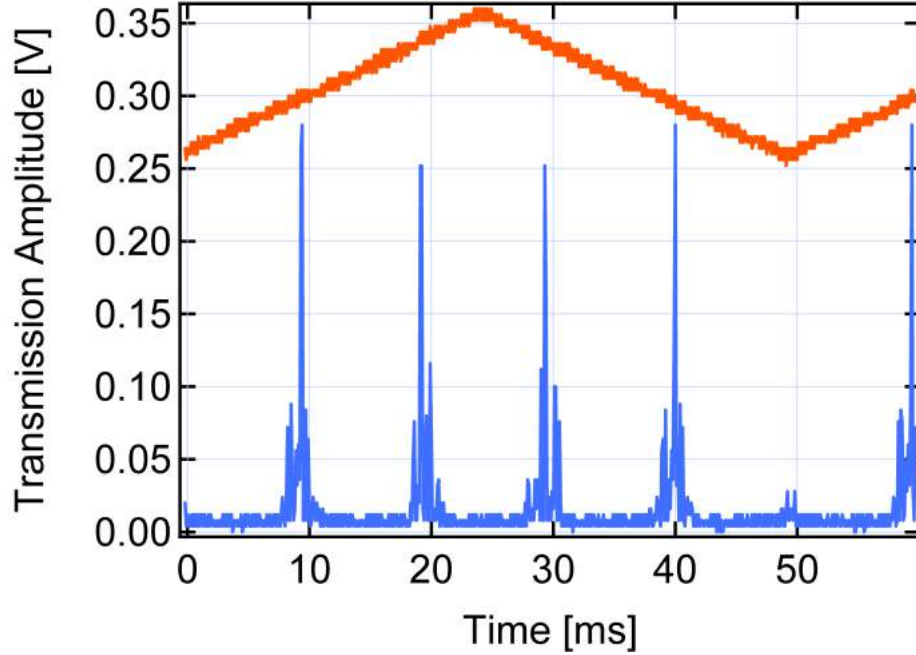


Figure 4.2: Passive cavity resonances with the electro-optic phase modulator turned on. Note that because the electro-optic phase modulator has transferred some of the carrier power into the sidebands (which are almost completely reflected from the reference cavity) the resonance peaks are smaller here than in figure 4.1. The red trace represents the scan driving voltage of the slow piezo, and is 10 Hz and  $2 V_{pp}$  (red curve not to scale).

power spectral density of the phase noise was taken to quantify the degree of timing jitter suppression (see equation 2.16 for the relationship between the PSD for phase noise and timing jitter). The phase noise measurement setup described in section 4.2.1 was used to characterize the phase noise of both the reference cavity-locked and free-running 500 MHz modelocked laser.

#### 4.2.1 Phase Noise Measurement Setup

The phase noise of a laser may be directly measured on the available PXA signal analyzer (Keysight N9030A), however, due to the limited dynamic range of the PXA signal analyzer, the phase noise floor of the modelocked 500 MHz laser is below the phase noise floor of the PXA signal analyzer above  $\approx 1$  kHz, which is ultimately limited by the stability of the

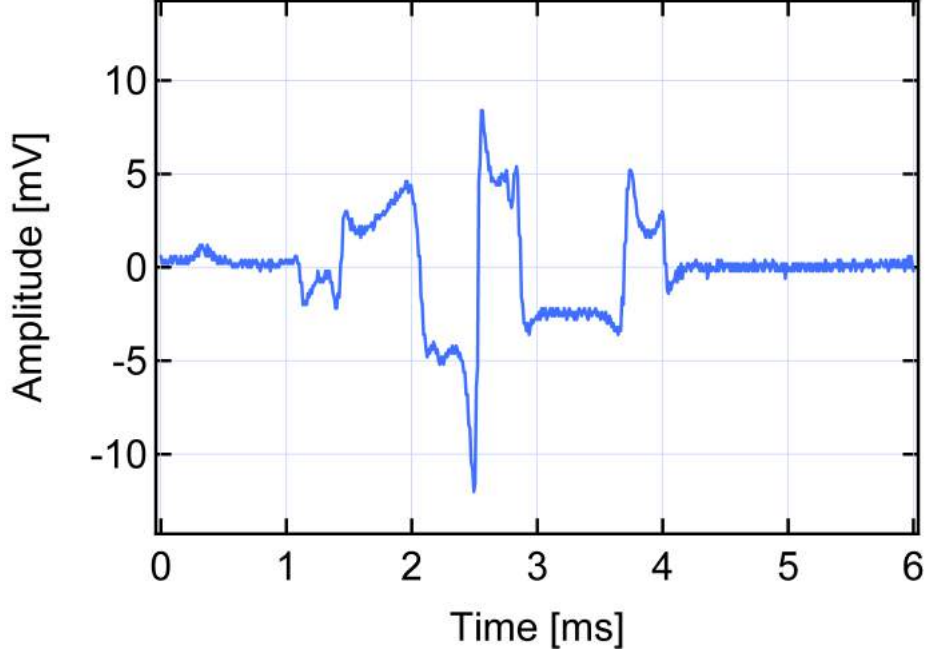


Figure 4.3: The experimental PDH error signal as visualized on an oscilloscope while scanning the laser cavity near resonance. The lock point is at 0 V. Note that the slope is steepest at the central lock-point (zero-crossing), this point corresponds to the largest resonance of the passive reference cavity. The asymmetry across the x-axis is caused by a non-uniform scan, which is likely reflective of a smaller amount of jitter of the repetition rate of the laser.

instrument's internal oscillator, as well as conversion losses and  $\frac{1}{f}$  noise from measuring at the RF carrier frequency. Therefore, a method which utilizes a more stable external oscillator was used to perform the final phase noise measurements. In this method, an ultra-stable monolithic modelocked laser with a 1 GHz repetition rate, which was designed and constructed in the Schibli Lab, was used as the ultra-stable oscillator (shown in figure 4.5).

The free-running 500 MHz modelocked laser measurement was performed by first obtaining a repetition rate-doubled carrier via the interleaver described in section 3.2.6. This was necessary to obtain a carrier which matched the 1 GHz carrier of the monolithic modelocked laser. Then, the output of this interleaver was coupled into a fiber which was subsequently converted to an electrical, RF signal via a fast photodiode and RF amplifier. This RF signal was then used as the RF modulation input of a dual-output electro-optic

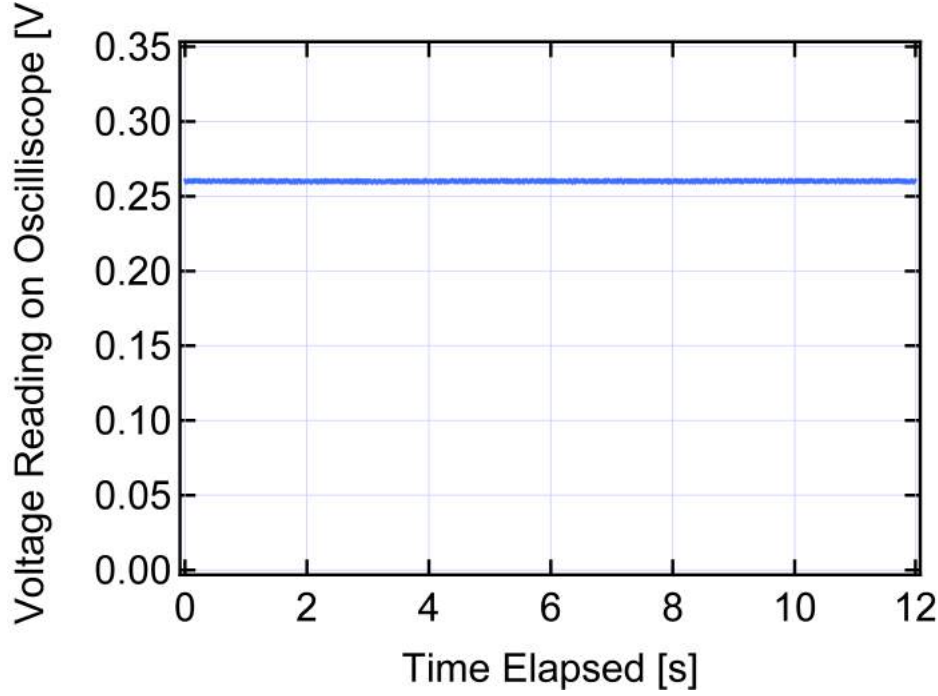


Figure 4.4: The transmission signal through the reference cavity with lock engaged for a period of 12 s. Note that the steady transmission signal roughly corresponds to the maximum resonance peak in figure 4.2.

intensity modulator, where light from the ultra-stable monolithic modelocked laser was coupled into both arms of the modulator. The electro-optic intensity modulator's two outputs were then shone onto two photodiodes which made up a balanced detector. Then, the power on each photodiode of the balanced detector was adjusted such that the signal from the detector was exactly zero when no RF power was applied. Then, the RF power (i.e. the interleaved 1 GHz carrier from the 500 MHz modelocked laser whose noise was to be measured) was applied and the two lasers loosely locked together via a low bandwidth PI feedback loop. This zero-crossing lock essentially enforced a 90 degrees relative phase difference between the pulses from the monolithic and the 500 MHz modelocked lasers. Due to the operation of the dual-output electro-optic intensity modulator, light would only exit the modulator when a ( $\approx 100$  fs) light pulse from the monolithic modelocked laser was present. This essentially provided a regular sampling rate of the RF power present on the modulator. Therefore, if

the 1 GHz carrier from the 500 MHz modelocked laser was completely noiseless, the balanced detector's signal would remain exactly at zero, as the carriers would never be present in the modulator at the exact same time (due to the aforementioned relative phase). However, any noise in the RF signal would be picked-up by the balanced detector and read by the PXA signal analyzer as phase noise, or equivalently and perhaps more intuitively here, timing jitter. In this sense, the electro-optic intensity modulator acts to mix the two carriers down to DC. Although a DC block had to be placed on the PXA signal analyzer to prevent damage during DC-coupling operation, the corner of the block was chosen to be 4 Hz to allow the method to pick up any phase noise above this frequency. By mixing the carrier down to DC, rather than measuring the phase noise directly at the RF carrier frequency, the PXA signal analyzer needed a smaller dynamic range ( $\approx 100$  dB less) to measure a much lower phase noise floor. In summary, the phase noise method used here did not aim to improve the dynamic range of the measurement instrument itself, but rather reduced the requirement of the PXA analyzer's dynamic range by almost fully removing the carrier. A block diagram of the phase noise measurement setup is provided in figure 4.5 for clarity.

Note that by mixing the carrier down to DC, the double-sided PSD is wrapped around to become a single-sided (double-sideband) phase noise PSD (i.e.  $S_\phi(f)$ ). The current standard for reporting a microwave carrier phase noise PSD is  $\mathcal{L}(f)$ , which is one-half of the double-sideband spectral density of phase noise, and is mathematically defined by IEEE standards as [35]:

$$\mathcal{L}(f) \equiv \frac{1}{2} S_\phi(f) \quad (4.1)$$

Thus, the data obtained from this measurement was adjusted by 3 dB to finally obtain  $L(f)$ . Furthermore, the data was scaled by the RF carrier power to yield the final units of  $\frac{\text{dBc}}{\text{Hz}}$ , the phase noise power in decibels, relative to the carrier power.



### 4.2.2 Phase Noise Measurement Results

The final results for the phase noise measurements described above are presented in figure 4.6. The measured phase noise PSD for the free-running (blue) and reference cavity locked (red) 500 MHz modelocked laser shows a significant improvement ( $\approx 20$  dB) in phase noise for the reference cavity-locked measurement from  $\approx 100$  Hz to  $\approx 1.1$  kHz. However, these phase noise measurements also appear to show that the 500 MHz modelocked laser locked to the reference cavity had a *higher* level of phase noise at frequencies below  $\approx 100$  Hz, but this is speculated to be a result of the larger bandwidth of this measurement's direct lock to the monolithic ultra-stable oscillator compared to the indirect lock used for performing the reference cavity-locked phase noise measurement, and in which case, could be regarded as an artifact of measurement. Furthermore, the peaks at  $\approx 14$  kHz and 600 kHz indicate that the measurement floor was limited in some way by the relative intensity noise (RIN) of the monolithic laser, as the measured RIN peaks of this laser match those seen in the phase noise data results. The exact cause of this limitation is still under investigation, but is possibly due to a resonance property of the dual-output EOM used in this measurement setup. The integrated timing jitter (from 100 Hz to 10 MHz) was 173.11 fs for the free-running 500 MHz modelocked laser and 46.91 fs for the reference cavity-locked 500 MHz modelocked laser over the same integration interval - an improvement by a factor of  $\approx 4$ . This data indicates that even with the basic, free-space, relatively low-finesse reference cavity used in this setup, the lock was very capable of reducing the phase noise due to acoustic vibrations. This is likely a result of the fact that the passive reference cavity has far less components (i.e. only two mirrors and their mounts) than the modelocked laser cavity, thus through the PDH lock demonstrated in this thesis, the reference cavity was able to transfer this increased acoustic stability to the 500 MHz modelocked laser. This reduction in the phase noise, and hence the timing jitter, at these frequencies is noteworthy given that this experimental setup was relatively non-complex and circumvents the long-term stability issues associated with

dedicated continuous-wave stabilization lasers, self-referencing  $f$  to  $2f$  schemes and ultra-stable microwave oscillators.

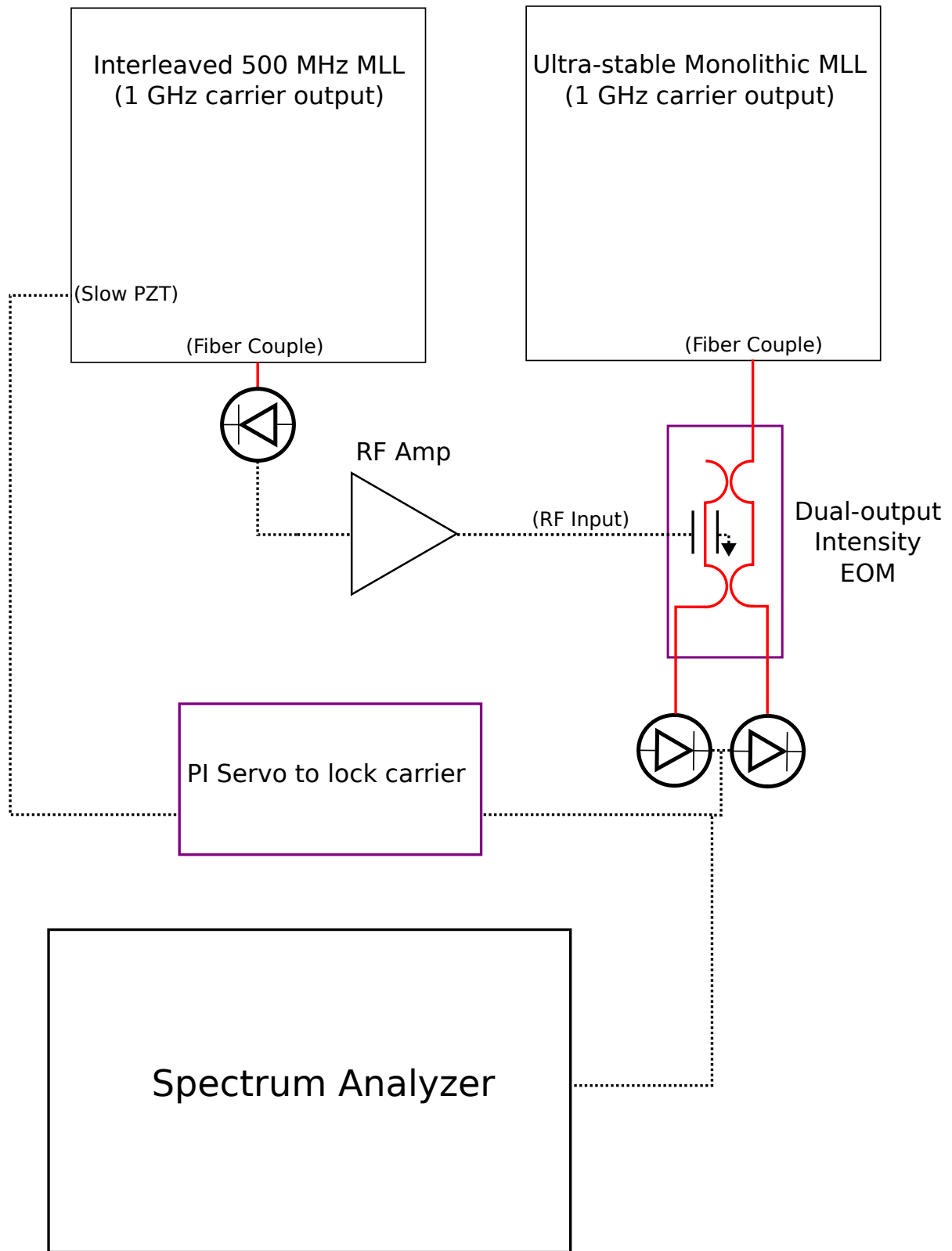


Figure 4.5: A block diagram for the phase noise measurement scheme described in section 4.2.1. The red solid lines represent beam (in fiber) paths and the dashed black lines represent electrical connections.

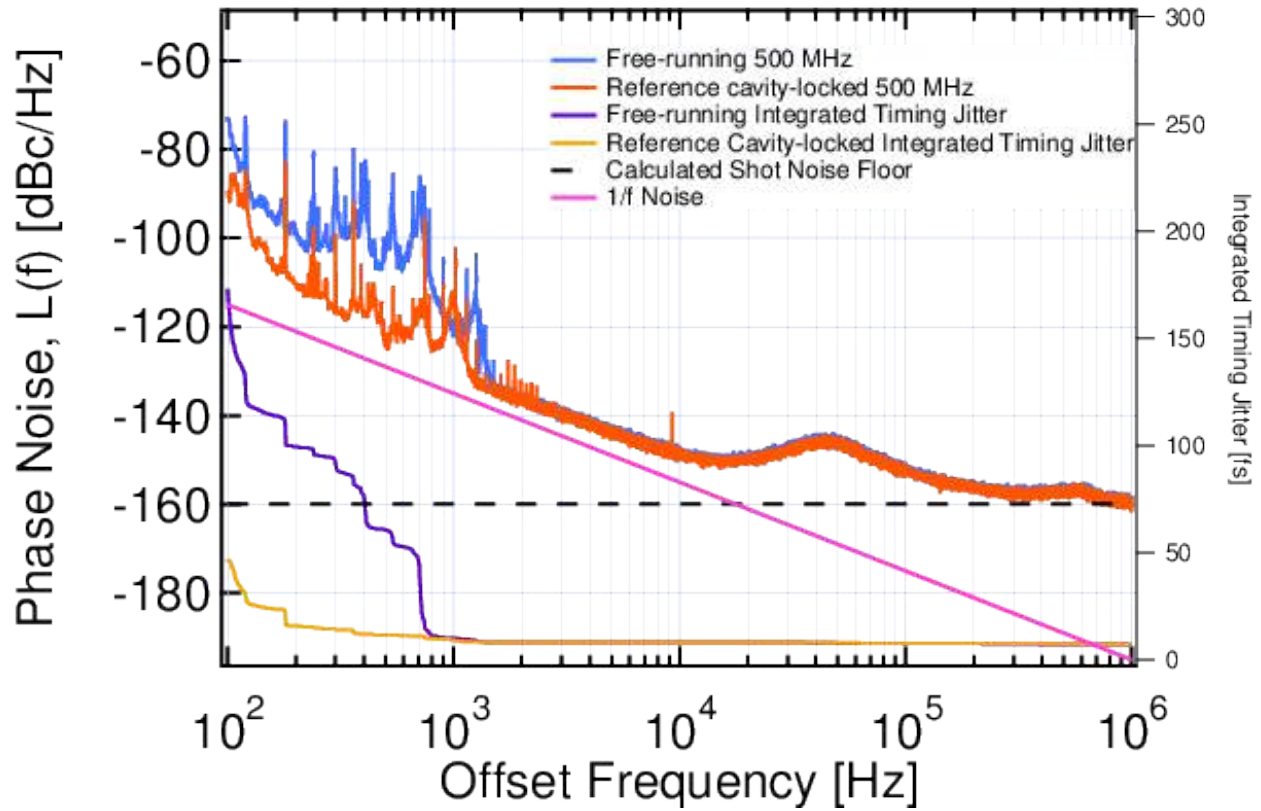


Figure 4.6: The phase noise measurement results, with a 1 GHz carrier, using the method described in section 4.2.1. The integrated timing jitter (from 100 Hz to 10 MHz) was 173.11 fs for the free-running 500 MHz modelocked laser and 46.91 fs for the reference cavity-locked 500 MHz modelocked laser over the same integration interval.

## Chapter 5

### Conclusion and Future Outlook

#### 5.0.1 Conclusion

In chapter 1 of this thesis, the applications of frequency combs generated by stable modelocked lasers were presented to provide a motivation for the development of modelocked laser stabilization techniques which would be helpful in furthering the goals of these applications. Namely, that better-stabilized frequency combs allow for increased precision, accuracy and scope of utility in the currently flourishing areas of frequency metrology, microwave generation and spectroscopic measurements. Then, in chapter 2, the origin of different types of noise in both continuous-wave and modelocked lasers were discussed in detail, including the coupling of common types of laser noise to timing jitter noise - of particular importance to the aforementioned applications. Next, in chapter 3, several established methods used to stabilize, and hence, reduce noise in both continuous-wave and modelocked lasers were discussed in detail. In the final sections of chapter 3, the famous Pound, Drever, Hall (PDH) method for the linewidth stabilization of continuous-wave lasers was adapted for the purpose of reducing the timing jitter of a modelocked laser and introduced as a method to achieve a balance between the great complexity involved with the previously mentioned established modelocked laser stabilization techniques and the instability associated with a completely free-running, free-space modelocked bulk laser. Lastly, in chapter 4, the efficacy of this method was demonstrated through measured timing jitter data from the application of this technique to a bulk, free-space modelocked Er:Yb laser. A deficiency of the technique introduced in this thesis

was the lack of carrier-envelope offset frequency stabilization, however timing jitter noise data obtained from the application of this method to stabilize a free-space modelocked Er:Yb laser indicated that this deficiency had relatively minor consequences for the ability of the method to reduce timing noise in the laser's output. Despite the absence of carrier-envelope offset frequency stabilization, the relatively non-complex and robust technique introduced in this thesis was ultimately successful in reducing the phase noise, and therefore the timing jitter, of a modelocked, free-space, bulk Er:Yb laser up to at least a 1.1 kHz offset frequency from the 1 GHz carrier. Due to the presence of a higher-than-expected noise floor using the phase noise measurement setup described in section 4.2.1, the degree of noise suppression above a 1.1 kHz offset frequency is unknown at this time. However, from the final timing noise measurements (figure 4.6) presented in this thesis, the technique clearly demonstrates its ability to achieve significant improvements in the timing noise of free-space modelocked lasers, while maintaining a high level of robustness and stability - potentially allowing for increased field-deployability in applications which require reduced timing jitter at acoustic frequencies. The ability of the method introduced in this thesis to reduce the timing noise of a *bulk, free-space* modelocked laser is particularly attractive as these types of lasers can provide important advantages over their fiber-based counterparts in many applications.

### 5.0.2 Future Study

Although the technique presented in this thesis was ultimately successful in reducing the phase noise and hence, timing jitter, of a bulk, free-space modelocked laser at lower-range acoustic frequencies, the setup could very likely be significantly improved by utilizing a higher-finesse passive reference cavity. The locking method introduced in this thesis would benefit from the higher finesse of this cavity by enabling a steeper discriminator slope in the error signal which is fed into the servo loop filter. In turn, this increased discriminator slope would allow the feedback loop to respond to even smaller drifts in frequency (the thermal-related frequency drifts of the reference cavity itself could be reduced if it were

placed in a vacuum), which would help to lower the magnitude of phase noise at even higher frequencies than the current setup. Furthermore, using a better isolated passive reference cavity, such as one made from a material with a low thermal expansion coefficient (e.g. propriety materials with ultra-low thermal expansion), would likely drastically decrease the acoustic noise within the reference cavity, allowing for the further suppression of phase noise at acoustic frequencies. Placing the entire reference cavity into a vacuum chamber would further decrease the noise present in the cavity - increasing the ability of the locking method to suppress phase noise. However, utilizing a vacuum chamber would also have the downside of adding a great deal of cost and fragility to the setup. In addition, an improved phase noise measurement of the Er:Yb laser stabilized with this technique - by using either a state-of-the-art measurement instrument with an ultra-stable oscillator or an improved measurement workaround - would allow for a more in-depth characterization of the strengths and shortcomings of this technique, thus fully revealing the current timing noise-suppression abilities and allowing for more directed efforts (with the above proposed alterations) in improving the technique. In summary, if future additional resources are allocated to improving the technique introduced in this thesis, a plethora of approaches are available which could further augment the timing jitter suppression ability of this method.

## References

- [1] L. E. Hargrove, R. L. Fork, and M. A. Pollack, "Locking of hene laser modes induced by synchronous intracavity modulation," Applied Physics Letters, vol. 5, no. 1, pp. 4–5, 1964.
- [2] R. Paschotta, "Noise of mode-locked lasers (Part I): numerical model," Applied Physics B, vol. 79, no. 2, pp. 153–162, 2004.
- [3] R. Paschotta, "Carrier-envelope Offset," Encyclopedia of Laser Physics and Technology.
- [4] J. Ye and S. T. Cundiff, Femtosecond Optical Frequency Comb: Principle, Operation, and Applications. 2005.
- [5] W. C. Swann, E. Baumann, F. R. Giorgetta, and N. R. Newbury, "Microwave generation with low residual phase noise from a femtosecond fiber laser with an intracavity EOM," CLEO: 2011 - Laser Science to Photonic Applications, vol. 19, no. 24, pp. 1–2, 2011.
- [6] S. Grop, P.-Y. Bourgeois, R. Boudot, Y. Kersale, E. Rubiola, and V. Giordano, "10 GHz cryocooled sapphire oscillator with extremely low phase noise," Electronics Letters, vol. 46, no. 6, p. 420, 2010.
- [7] F. Quinlan, T. M. Fortier, M. S. Kirchner, J. a. Taylor, J. C. Bergquist, T. Rosenband, N. Lemke, a. Ludlow, Y. Jiang, C. W. Oates, and S. a. Diddams, "Optical frequency combs for low phase noise microwave generation," 2011 XXXth URSI General Assembly and Scientific Symposium, vol. 1, pp. 1–3, 2011.
- [8] A. Marian, M. C. Stowe, D. Felinto, and J. Ye, "Direct frequency comb measurements of absolute optical frequencies and population transfer dynamics," Physical Review Letters, vol. 95, no. 2, pp. 1–4, 2005.
- [9] T. R. Schibli, "Frequency combs: Combs for dark energy," Nature Photonics, vol. 2, no. 12, pp. 712–713, 2008.
- [10] T. Steinmetz, T. Wilken, C. Araujo-hauck, R. Holzwarth, W. Hänsch, L. Pasquini, A. Manescau, S. D. Odorico, M. T. Murphy, T. Kentischer, W. Schmidt, and T. Udem, "Laser Frequency Combs for Astronomical Observations Laser Frequency Combs for Astronomical Observations," Science (New York, N.Y.), vol. 1335, no. September, pp. 1335–7, 2008.






- [11] R. Paschotta, “Laser Noise,” Encyclopedia of Laser Physics and Technology.
- [12] R. Paschotta, “Noise in Laser Technology (Part 1),” Optik & Photonik, vol. 4, no. 2, pp. 48–50, 2009.
- [13] R. Paschotta, “Power Spectral Density,” Encyclopedia of Laser Physics and Technology.
- [14] R. Paschotta, “Relaxation Oscillations,” Encyclopedia of Laser Physics and Technology.
- [15] R. Paschotta, “Frequency Noise,” Encyclopedia of Laser Physics and Technology.
- [16] A. L. Schawlow and C. H. Townes, “Infrared and optical masers,” Physical Review, vol. 112, no. 6, pp. 1940–1949, 1958.
- [17] R. Paschotta, “Derivation of the Schawlow-Townes Linewidth of Lasers,” The Encyclopedia of Laser Physics and Technology, pp. 1–6, 2013.
- [18] R. Paschotta, “Self-heterodyne Linewidth Measurement,” Encyclopedia of Laser Physics and Technology.
- [19] R. Paschotta, “Passive Mode Locking,” Encyclopedia of Laser Physics and Technology.
- [20] R. Paschotta, “Mode Locking,” Encyclopedia of Laser Physics and Technology.
- [21] H. A. Haus and A. Mecozzi, “Noise of Mode-locked Lasers,” IEEE Journal of Quantum Electronics, vol. 29, no. 3, pp. 983–996, 1993.
- [22] H. A. Haus, J. G. Fujimoto, and E. P. Ippen, “Structures for additive pulse mode locking,” Journal of the Optical Society of America B, vol. 8, no. 10, p. 2068, 1991.
- [23] R. Paschotta, “Noise of mode-locked lasers (Part II): timing jitter and other fluctuations,” Applied Physics B-Lasers and Optics, vol. 79, pp. 163–173, 2004.
- [24] R. Paschotta, “Noise in Laser Technology (Part 3),” Optik & Photonik, vol. 4, no. 2, pp. 48–50, 2009.
- [25] Y. Fei, “Thermal expansion,” Rock Physics and Phase Relations, pp. 29–44, 1995.
- [26] J. T. Verdeyen, Laser electronics. Prentice-Hall, 2 ed., 1989.
- [27] K. Hiremath, “Finesse and quality factor.”
- [28] R. W. P. Drever, J. L. Hall, F. V. Kowalski, J. Hough, G. M. Ford, A. J. Munley, and H. Ward, “Laser phase and frequency stabilization using an optical resonator,” Applied Physics B, vol. 31, no. 2, pp. 97–105, 1983.
- [29] A. White, “Frequency stabilization of gas lasers,” IEEE Journal of Quantum Electronics, vol. 1, no. 8, pp. 349–357, 1965.
- [30] E. D. Black, “An introduction to PoundDreverHall laser frequency stabilization,” American Journal of Physics, vol. 69, no. 1, p. 79, 2001.

- [31] T. W. Hansch and B. Couillaud, “Laser frequency stabilization by polarization spectroscopy of a reference cavity,” Optics Communications, vol. 35, no. 3, pp. 441–444, 1980.
- [32] D. J. Jones, S. A. Diddams, J. K. Ranka, A. Stentz, R. S. Windeler, J. L. Hall, and S. T. Cundiff, “Carrier-Envelope Phase Control of Femtosecond Mode-Locked Lasers and Direct Optical Frequency Synthesis,” Science, vol. 288, no. 5466, pp. 635–639, 2000.
- [33] R. Paschotta, “ABCD Matrix,” Encyclopedia of Laser Physics and Technology.
- [34] E. P. Ippen, “Principles of passive mode locking,” Applied Physics B Laser and Optics, vol. 58, no. 3, pp. 159–170, 1994.
- [35] J. R. V. (Chairman), (IEEE Standard 1139-1999) IEEE Standard Definitions of Physical Quantities for Fundamental Frequency and Time Metrology - Random Instabilities. 1999.

## Appendix A

### Kigre Inc. Erbium-doped Ytterbium Glass, QX/Er Datasheet<sup>1</sup>

<div style="display: flex; justify-content: space-between; align-items: center;">  <div style="text-align: center;">  <b>KIGRE, INC.</b> </div>  </div> <p style="text-align: center;"><b>QX LASER GLASSES</b></p> <p style="text-align: center;">These phosphate glass laser materials exhibit a chemical durability that is comparable to silicate glasses. QX glasses are designed to withstand high thermal loading and shock</p>			
PROPERTIES	QX/Nd	QX/Er	QX/Yb
Laser Wavelength Peak (nm)	1054	1535	1032
Emission Cross Section ( $\times 10^{-20} \text{cm}^2$ )	3.8	0.8	0.4
Absorption Cross Section ( $\times 10^{-20} \text{cm}^2$ )	0.7	1.7@977nm	1.4
Fluorescence Lifetime (us)	353	7900	2000
Fluorescence Linewidth (nm) FWHM	27.6	55.0	56.5
Index of Refraction ( $n_D$ )	1.538	1.532	1.535
( $n_F$ )	1.543		
( $n_C$ )	1.536		
( $n_F$ ) - ( $n_C$ ) ( $\times 10^{-5}$ )	815	848	834
Abbe Number	66.0	63.7	61.1
Index of Refraction (laser line)	1.53	1.521	1.52
$dn/dt$ (20-40 °C) ( $\times 10^{-7}/^\circ\text{C}$ )	-4	-21	-21
Thermo-stress Birefr. Coeff. $Q = [E/2(1-\mu)] (C_1 - C_2)$ ( $\times 10^{-7}/^\circ\text{C}$ )	9.0	9.1	9.1
Thermo-optical Coeff. $W = [dn/dt + (n-1)] (\times 10^{-7}/^\circ\text{C})$ @ 70°C	59	41	41
Thermo-optical Coeff. $W = [dn/dt + (n-1)] (\times 10^{-7}/^\circ\text{C})$ @ 30°C	51	33	33
Transformation Temperature (°C)	506	470	450
Deformation Temperature (°C)	535	502	485
Coeff. of Thermal Expansion (20-40°C) ( $\times 10^{-7}/^\circ\text{C}$ )	72	76	83
(20-100 °C)	84	88	95
(20-300 °C)		99	
Nonlinear Index $n_2$ ( $\times 10^{-13}$ esu)	1.17	1.22	1.22
Density (g/cc)	2.66	2.93	2.81
Thermal Conductivity (W/mK)	0.85	0.85	0.85
Young's Modulus ( $\times 10^{11}$ N/mm <sup>2</sup> )	71	67	67
Poisson's Ratio	0.24	0.24	0.24
Stress Optical Coeff. $B = [C_1 - C_2] (\times 10^{-6} \text{ mm}^2/\text{N})$	2.1	2.3	2.3
Stress Thermal-Optical Coeff. "P" ( $\times 10^{-6}/\text{K}$ ) $P = dn/dt - (E/2(1-\mu)) (C_1 + 3C_2)$	-3.6	5.1	5.1
Knoop Hardness (kgf/mm <sup>2</sup> )	503	435	435
Durability (Wt. loss $\times 10^{-5}$ g/cm <sup>2</sup> , H <sub>2</sub> O, 100°C, 1Hr)	5.0	5.2	5.2
ED <sub>2</sub> Q-246, = $5.5 \times 10^{-5} \text{ g/cm}^2$			
Thermal Loading Limit, TTL (watts/inch) (unstrengthened)	> 300	> 150	> 300
LAMP PUMPED (strengthened)...5x80mm rod	> 900	> 450	> 900
LAMP PUMPED (strengthened)...10x150mm rod	> 500	> 250	> 500

conditions in both ion-exchanged strengthened and un-strengthened configurations.

Note: TTL = Rupture Strength. Unstrengthened QX glasses exhibit a Rupture Strength of ~ 10,000 psi. Strengthened QX glasses exhibit a Rupture Strength of ~ 40,000 psi.. The TTL is strongly dependent upon rod barrel surface conditions.

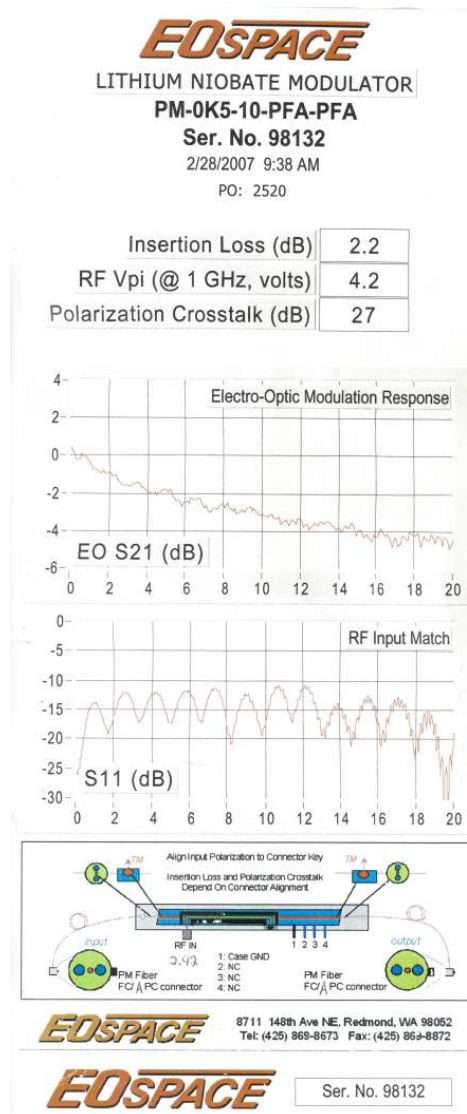
Wt% to ions/cc: Wt%(g)/100g  $\times$  2.9g/cc  $\times$  2  $\text{Er}^{3+}/382.52\text{g/mole} \times 6.02 \times 10^{23}$  ions/mole = ions/cc  $\text{Er}^{3+}$

PHONE: (843) 681-5800 FAX: (843) 681-4559  
E-MAIL: info@kigre.com

<sup>1</sup>Datasheet provided by Kigre, Inc. - Reproduced here with permission.

## Appendix B

### Fiber-Based Lithium Niobate EOM-PM Datasheet<sup>1</sup>

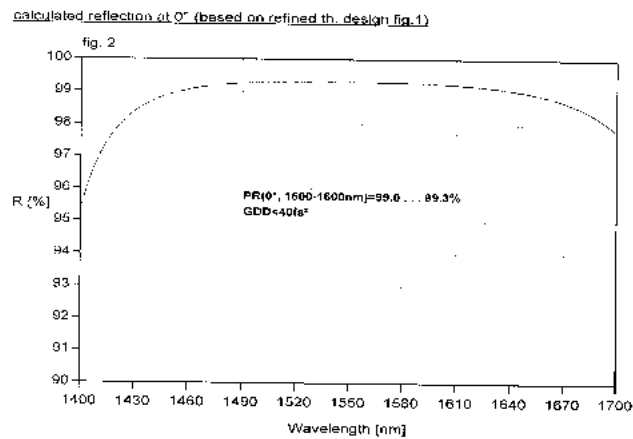
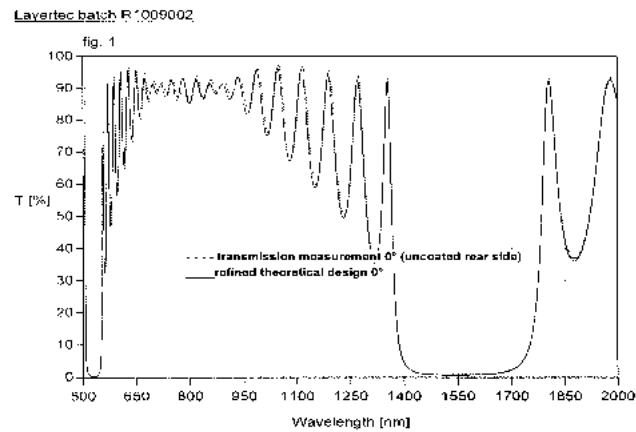


<sup>1</sup>Datasheet provided by EOSpace - Reproduced here with permission.

## Appendix C

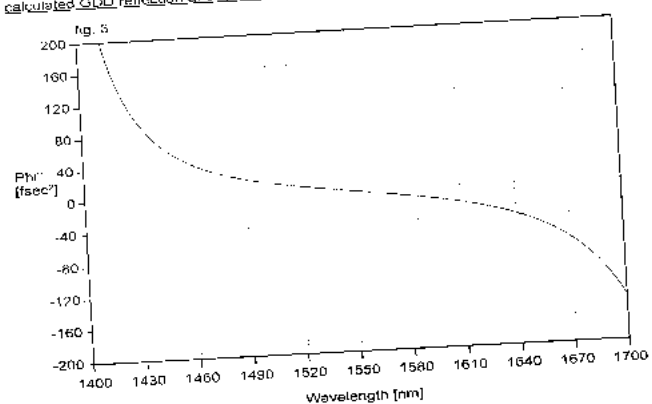
### Layertec Mirror Dielectric Coating Datasheets<sup>1</sup>

$r = 500$  mm (Article #: 108475, Coating Batch: R1009002):

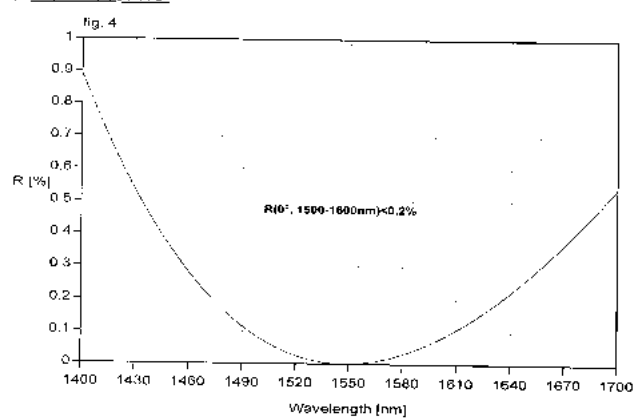


<sup>1</sup>Datasheets provided by Layertec, GmbH. - Reproduced here with permission.

calculated GDD reflection at 0° (based on refined th. design fig. 1)



theory rear side AR 0°



$r = 1000 \text{ mm}$  (Article #: 109332, Coating Batch: F115H010):

fig. 1: transmission measurement (---), recalc. theoretical design (—) - S2

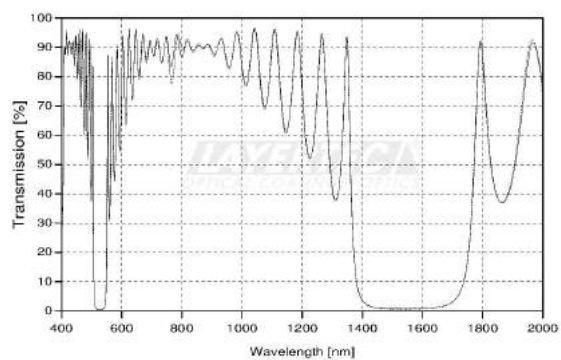


fig. 2: calculated reflection from recalc. design shown in fig. 1

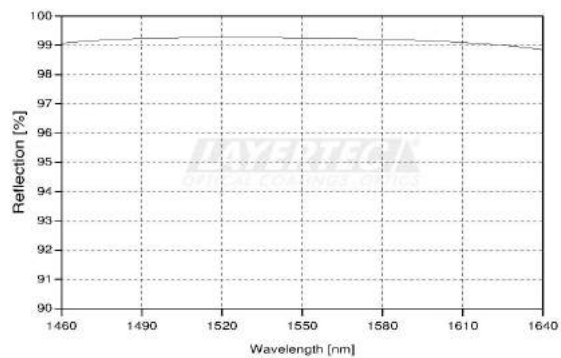


fig. 3: calculated GDD from recalc. design shown in fig. 1

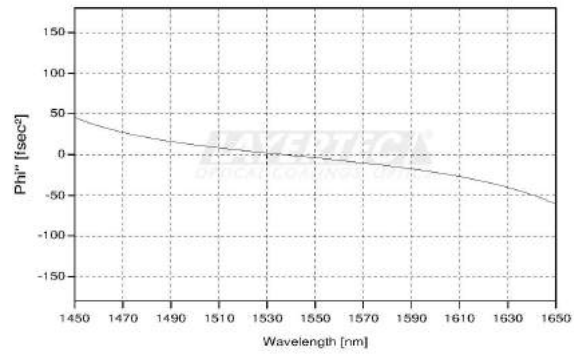


fig. 4: calculated reflection of the theoretical design of S1

